Mean field model and statistical properties of a 6 layered neocortical network

Csaba Erő

Henry Markram, Supervisor
Athanassia Chalimourda, Assistant
Jean-Pascal Pfister, External expert

École Polytechnique Fédérale de Lausanne
(EPFL)
2012-2013

Contents

Previous work has shown that mean-field models are well suited to describe the ensemble firing rates of cortical network with dynamic synapses (Sussillo D., Toyoizumi T., & Maass W. (2007); Tsodyks M., Pawelzik K., & Markram H. (1998)). In this project we want to apply the mean-field methods outlined in these and other papers to the neocortical column, reconstructed in the Blue Brain Project and to investigate the statistical and dynamical properties of the resulting network architecture. The project will start from the connectivity data of the BBP neocortical column and two population mean-field model of cortical firing rates. The first step is to extend the mean-field model to 55 morphologically sorted neuronal populations coupled by a 55 dimensional connectivity matrix and accordingly many populations of dynamic synapses. Finally, the influence of synaptic plasticity and learning on the network dynamics are investigated. The plausibility of the mean field model will be monitored by comparing it to detailed simulations of the corresponding neocortical column. The investigation of the model will mainly use numerical methods and computer simulations.

1 Introduction

One of the main complexities of the human brain lies in its incredible amount of cells that all interact with each other, participating in the global activity of the system. This leads to a wide range of possible behaviors which, despite multiple efforts, could still not be completely reproduced and understood. The task of doing so is very complex, not only because of the lack of understanding of the exact rules that are responsible for the plastic changes in such a high dimensional network, but also because of the limitations of the currently existing computational power at disposal for simulating such networks.

One approach to deal with the latter, are *mean-field* models. These are based on the assumption that the firing rate of similarly connected neurons can be computed by a few equationswhich describe the average of the entire population, rather than simulating each cell individually. This greatly reduces the computational complexity, since the number of connections in the network drastically as the number of nodes to simulate decreases.

The validity of this approach depends on the level of detail desired for the final behavior model. While mean-field models do not account for local and short-term interactions between single neurons, they give a good approximation of the rate evolution of populations composed of a large number of cells.

The cortex is a good example of a large network with layer- and morphology-wise repartition of the neurons. In this project, we used the mean-field model described by Tsodyks M., Pawelzik K. and Markram H. to model the firing rates of the 6 layered neocortical column network provided by the Blue Brain Project (BBP).

For computational reasons, we developed the mean-field model based on the results of a point-neuron model of the BBP column. The same approach can, however, be used to obtain a mean-field model of the original BBP column.

We developed a calibration procedure which determines the connection parameters, a neural rate transfer function as well as other parametersof the population model from the BBP column.

The plausibility of the mean-field model was tested by comparing the firing rate evolution of the 2 models, and pointing out the main problems that this simplification encounters. It was furthermore shown that certain tasks such ball balancing, simple enough to be learned by the mean-field populations, could be transfered to the cortical column without the need to modify the synaptic weights again.

This procedure would therefore show the possibility of reducing a complex biological system into a much smaller network, while keeping its overall behavior.

2 Synapse and neuron models

In this project, we studied different synapse models, starting from the original Tsodyks-Markram synapse to its mean-field formulation. The biological origins and the mathematical description of the different models will be explained in this section.

The adaptive exponential integrate-and-fire (AdEx) neuronal model (Brette R., Gerstner W. (2005)) for point-neuron simulations will also be described.

2.1 Tsodyks-Markram synapse model

In order to be able to compute the dynamics of a complex network - such as the cortex - it is vital to have a good description of its neural dynamics. One has to describe in the most accurate way possible the mechanisms that underlie the propagation of information through the wide range of synapses that connect the neurons of the network.

The first model of interest in this project was described by Tsodyks and Markram (1997) and Abbott et al. (1997). It reproduces well the synaptic dynamics between pyramidal neurons. This model supposes that all synapses are characterized by their amount of available resources at a given time. The available resources are divided into 3 possible states x, y and z, corresponding to the recovered, active, and inactive states respectively. Each presynaptic spike activates a certain fraction U_{SE} (**u**tilization of **s**ynaptic **e**fficacy) of available resources x, thereby depleting them. The depleted resources go into active state y and start inactivating with a time constant τ_{in}. They then go into inactive state z. From the inactive state y, the available resources recover gradually back to the available state x, with a time constant τ_{rec}. Their evolution in time can be described by the following set of equations:

$$\begin{aligned} \frac{dx}{dt} &= \frac{z}{\tau_{rec}} - U_{SE} \cdot x(t_{sp} - 0) \cdot \delta(t - t_{sp}) \\ \frac{dy}{dt} &= -\frac{y}{\tau_{in}} + U_{SE} \cdot x(t_{sp} - 0) \cdot \delta(t - t_{sp}) \\ \frac{dz}{dt} &= \frac{y}{\tau_{in}} - \frac{z}{\tau_{rec}} \end{aligned} \tag{1}$$

where t_{sp} is the spike time. The postsynaptic current produced is proportional to the fraction of active resources y, such that

$$I_s(t) = A_{SE} \cdot y(t)$$

where A_{SE} is a constant. The mechanism from presynaptic spike to postsynaptic current can therefore be visualized as follows:

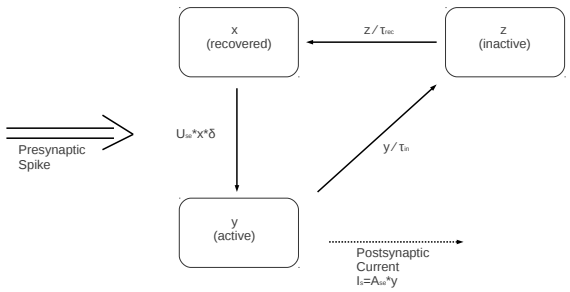

Figure 1: Mechanism from presynaptic spike to postsynaptic current in a Tsodyks-Markram synapse.

To also describe synaptic facilitation the fraction U_{SE} of resources is not constant anymore, but can increase by each incoming presynaptic spike and goes back to zero with a time constant τ_{fac}, as described by the following equation:

$$\frac{dU_{SE}}{dt} = -\frac{U_{SE}}{\tau_{fac}} + U_{SE}^0 \cdot (1 - U_{SE}) \cdot \delta(t - t_{sp}) \tag{2}$$

where U_{SE}^0 determines the increase of U_{SE} due to presynaptic spikes. Therefore if no or only a few presynaptic spikes occur, the variable U_{SE} stays near its steady value of $U_{SE} \approx 0$. However for a continuous set of spikes, U_{SE} is increased up to its maximal value of 1, provided that the rate of presynaptic spikes and the constant U_{SE}^0 are high enough to compensate for its decrease with a time constant τ_{fac}.

A large depressing time constant τ_{rec} leads to a slow recovery of resources whereas a low facilitating time constant τ_{fac} allows the fraction U_{SE} of resources to go down quickly to its resting value of zero. Thus a synapse is said to be depressing if τ_{rec} is much larger than its facilitating time constant τ_{fac}. The opposite is true for facilitating synapses, with a quick recovery of available resources and a fraction U_{SE} which can be maintained at a high value for different presynaptic input rates.

The model's ability to describe both facilitating and depressing synapses is vital, because of the various roles that these play in the network dynamics. For instance, the response of a depressing synapse is large to the first spike, but decreases fast once it gets activated. On the other hand, facilitating synapses give a weaker immediate response, which however increases with each new spike. This has consequences for the network activity propagation. Depressing synapses for example are optimal for information transmission at low rates (0.5-5 Hz) whereas facilitating synapses prefer higher presynaptic rates (9-70 Hz) (Fuhrmann G., Segev I., Markram H., Tsodyks M. (2001)).

Also, depressing synapses in a network allow for a higher sensitivity to lower input rates as their transmission efficiency decreases for higher rates (Abbott L, Varela J., Sen K., Nelson S. (1997)). They have also been shown to reduce autocorrelation in the transmitted information, and therefore lower redundancy (Goldman M., Maldonado P., Abbott L. (2002)).

2.2 Extension of the Tsodyks-Markram synapse model

The Tsodyks-Markram model describes synaptic dynamics well. However, equations-(1) can be brought to a simpler form.

Fuhrmann G., Segev I., Markram H., Tsodyks M. (2001) reduced all equations of (1) to only 2 equations. The first is the evolution of the fraction of available resources:

$$\frac{dx}{dt} = \frac{(1 - x)}{\tau_{rec}} - U_{SE} \cdot x \cdot \delta(t - t_{sp}) \tag{3}$$

Althought this variable x is similar to the previous variable of the same name in (1), its kinetics do not depend on any other variable besides its own value in case of no presynaptic spike. This equation shows that without any presynaptic spike, the fraction of available resources tends to go to its maximal value of $x_{max} = 1$, with a time constant τ_{rec}.

As in the previous equations, each incoming presynaptic spike activates a certain fraction U_{SE} of resources which to also describe facilitating synapses has to follow the same dynamics as in (1):

$$\frac{dU_{SE}}{dt} = -\frac{U_{SE}}{\tau_{fac}} + U_{SE}^0 \cdot (1 - U_{SE}) \cdot \delta(t - t_{sp}) \tag{4}$$

Again, the synapse can be described as depressing, if the resources x recover slowly and the fraction of resources used at a presynaptic spike U_{SE} goes quickly back to 0, hence $\tau_{rec} \gg \tau_{fac}$. The synapse is said to be facilitating in the opposite case, eg. $\tau_{rec} \ll \tau_{fac}$.

The synaptic current induced by a presynaptic spike at time $t = 0$ that flows into the neuron can then be written as

$$I(t) = U_{SE} \cdot x \cdot \bar{g} \cdot g_{norm}(t) \cdot (E - V) \tag{5}$$

$\bar{g}$ being the maximum synaptic conductance, $g_{norm}(t)$ the normalized time-dependent synaptic conductance, E the reversal potential and V the membrane potential of the neuron. The normalized time-dependent synaptic conductance $g_{norm}(t)$ is usually a superposition of exponential functions, and the reversal potential E is a characteristic of the synapse ($E_{exc} \approx 0$mV for excitatory and $E_{inh} \approx -75$mV for inhibitory synapses).

2.3 Adaptive exponential integrate-and-fire (AdEx) model

The adaptive exponential integrate-and-fire (AdEx) model is a 2-dimensional model that is composed of an exponential spike mechanism and an adaptation equation. It can predict on average up to 96% of the spikes with $2ms$ precision, if driven by realistic, conductance-based, synaptic inputs (Brette R. & Gerstner W. 2005).

Its main advantage is its simplicity, with only 2 equations per point-neuron, while giving more precise results than most other integrate-and-fire models. It is defined as

$$\begin{aligned} C\frac{dV}{dt} = \quad & -g_L(V - E_L) + g_L\Delta_T exp\left(\frac{V - V_T}{\Delta_T}\right) - g_e(t - t_{sp})(V - E_{exc}) - g_i(t - t_{sp})(V - E_{inh}) \\ & + I^{ext} - w \\ \tau_w\frac{dw}{dt} = \quad & a(V - E_L) - w \end{aligned} \tag{6}$$

C_m being the membrane capacitance, V_T the spike threshold and Δ_T the slope factor of the exponential term. Furthermore, E_L is the leak reversal potential, g_L the leak conductance and a the subthreshold adaptation. w is the adaptation current and τ_w is its corresponding time constant. E_{exc} and E_{inh} are the excitatory and inhibitory reversal potential respectively and finally $g_{exc}(t)$ and $g_{inh}(t)$ are respectively the total excitatory and inhibitory spike-triggered synaptic conductances in time.

After each spike, the membrane potential is reset to resting value E_L and the adaptation current w is incremented by an amount b such that

$$\begin{array}{cc} \text{At spike:} & \\ V & \rightarrow E_L \\ w & \rightarrow w + b \end{array}$$

To better understand the dynamics of the AdEx model, it is instructive to study the phase-plane of the variables V and w, for the case of different input currents (see figure-2). The figure shows the nullclines of V ($\frac{dV}{dt} = 0$) and w ($\frac{dw}{dt} = 0$), their intersections being a stable and unstable fixed-point.

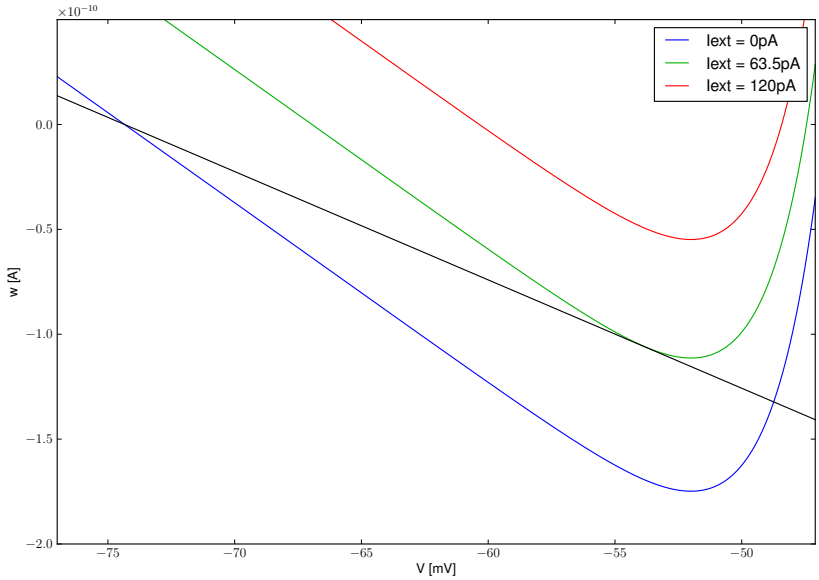

Figure 2: Phase plane representation of the AdEx neuron model with the nullclines of the two variables w (*straight line*) and V (*curved lines*), for the parameters shown in table-2. The intersections of the two nullclines result in a stable (*left*) and an unstable (*right*) fixed-point. As the external current is increased, the two fixed-points end up merging together and eventually disappear, resulting in a continously firing neuron.

2.4 Mean-Field Model

The disadvantage the previously seen methods is their high requirement in computational power when larger areas of the brain are simulated, such as a column of the neocortex as it is the case in this project. However, neurons of the same type with similar connectivities show a similar firing rate. It is therefore possible to compute the average rate for such populations of neurons, instead of computing the rate for each cell individually. This would reduce the computational costs, while still obtaining a good approximation of the behavior of the neural populations.

We will later describe how to determine the neural populations based on neuron type and connections.

The equations describing an average population activity are often called mean-field models. The model used here was developed by Tsodyks M., Pawelzik K. and Markram H. (1997). The equations of this mean-field model, take in account both depressing and facilitating connections and are described by

$$\begin{aligned} \frac{d\langle x\rangle}{dt} &= \frac{1-\langle x\rangle}{\tau_{rec}} - \langle U_{SE}\rangle \cdot \langle x\rangle \cdot F(t) \\ \frac{d\langle U_{SE}^{-}\rangle}{dt} &= -\frac{\langle U_{SE}^{-}\rangle}{\tau_{fac}} + U_{SE}^{0} \cdot (1 - \langle U_{SE}^{-}\rangle) \cdot F(t) \\ \langle U_{SE}\rangle &= \langle U_{SE}^{-}\rangle \cdot (1 - U_{SE}^{0}) + U_{SE}^{0} \end{aligned} \tag{7}$$

where $F(t)$ is the Poisson rate of a neuron population at time t, and $\langle U_{SE}^{-}\rangle$ is the average value of U_{SE} just before the spike.

When averaging equation-3 over different Poisson spike realizations, the assumption was made that the variables $x(t)$ and $U_{SE}(t)$ are statistically independent, ie.

$$\langle xU_{SE}\rangle = \langle x\rangle\langle U_{SE}\rangle \tag{8}$$

This is only the case if the synapse is not facilitating, as the variable $U_{SE}(t)$ will be a constant parameter of the model, and $x(t)$ will be function of the spike arrival times prior to the current time. It was shown (Tsodyks M., Pawelzik K. and Markram H. (1997)) that in all cases considered, the described mean-field model was still a good approximation, because the coefficient of variation of $U_{SE}(t)$ and $x(t)$ was very small, resulting in small statistical correlation between them.

The dynamics of a population with a large number of neurons that have similar receptive field properties can be described by the following equation (Sussillo D., Toyoizumi T., Maass W. (2007)):

$$\tau_m \frac{dF_i}{dt} = -F_i + h\left(\sum_j J_{i,j} \cdot y_{i,j} + I_i^{ext}\right) \tag{9}$$

where F_i is the rate of population i, τ_m is its membrane time constant, $h(I)$ its activation function, I_i^{ext} its external input, and $J_{i,j}$ the weight of the connection from population j to i. The variable y of equation-1 can be averaged similarly, yielding

$$\frac{d\langle y\rangle}{dt} = -\frac{d\langle y\rangle}{\tau_{in}} + \langle U_{SE}\rangle \cdot \langle x\rangle \cdot \langle F(t)\rangle \tag{10}$$

Further simplification assuming that τ_{in} is much faster than τ_{rec} allows to write

$$y(t) = F(t) \cdot \tau_{in} \cdot U_{SE} \cdot x \tag{11}$$

which is valid for cases where one is interested only in a timescale slower than τ_{in}. Equation-9 then becomes

$$\tau_m \frac{dF_i}{dt} = -F_i + h\left(\sum_j J_{i,j} \cdot \langle U_{SE}\rangle_{i,j} \cdot \langle x\rangle_{i,j} \cdot F_j + I_i^{ext}\right) \tag{12}$$

where τ_{in} was merged with the weight J for brevity. The dimensions and units of the variables and constants are given in table-3.

This equation therefore describes directly the evolution of the population rate, instead of the firing spikes, with the consequence that it is impossible to predict individual activities of neurons, in case that the interaction becomes local. Also, for different combinations of the parameters U_{SE}^0, τ_{rec} and τ_{fac}, the assumption of independence in equation-8 does not hold because of the high correlation between the variables $U_{SE}(t)$ and $x(t)$ and results in systematic errors in the firing rates.

For simplicity, the averaging signs $\langle\rangle$ on the variables of the model will be omitted in the rest of this report.

3 Different simulations

3.1 Whole column simulation

The first simulation was a detailed computation of the activity of the neocortical column neurons, based on network data created at the Blue Brain Project from biological measurements and consisting of multiple cortical columns side-by-side of compartmental neurons.

Althought this data could have been used in its original form in this project, it was too complex to simulate and thus reduced to a single column of point-neurons, by replacing the compartmental axons and dendrites by only a delay time to account for the propagation of action-potentials. The simulation of this reduced data was taken as a reference to be calibrated and compared with the results of the mean-field simulation.

The synapses were described by the extension of the Tsodyks-Markram model (equations 3 and 4), and the adaptive exponential integrate-and-fire model (AdEx) (equation-6) was used for the point-neurons, both of which were detailed earlier in this report.

3.1.1 Column Parameters

The simulated data contained 31000 point-neurons and roughly $3.5 \cdot 10^7$ synapses connecting them together, with different synaptic constants and delay times for spike propagation. There was thus a total of

$$3.5 \cdot 10^7 \cdot 2 + 31000 \cdot 2 \approx 7 \cdot 10^7$$

equations to compute at every step of the simulation. The data's biological origin was a cortical column, with a perpendicular orientation according to the layers. The neurons were layer-wise distinguished from each other, as shown in figure-3.

For every of the $3.5 \cdot 10^7$ synapses of the column, a set of synaptic parameters was given (see table-1), that allowed the computation of the extended Tsodyks-Markram synapse model equations 3 and 4.

Synapse Parameter	Unit	Description
g	nS	Maximal conductance
τ_{rec}	ms	Depression time constant
τ_{fac}	ms	Facilitation time constant
D	ms	Delay of transmission
U^0_{SE}	-	Step increase of fraction of resources used U_{SE}

Table 1: Synaptic constants given by the column dataset and their description.

For the AdEx model, 2 sets of parameters were used. One for all excitatory neurons and one for all inhibitory neurons (see table-2).

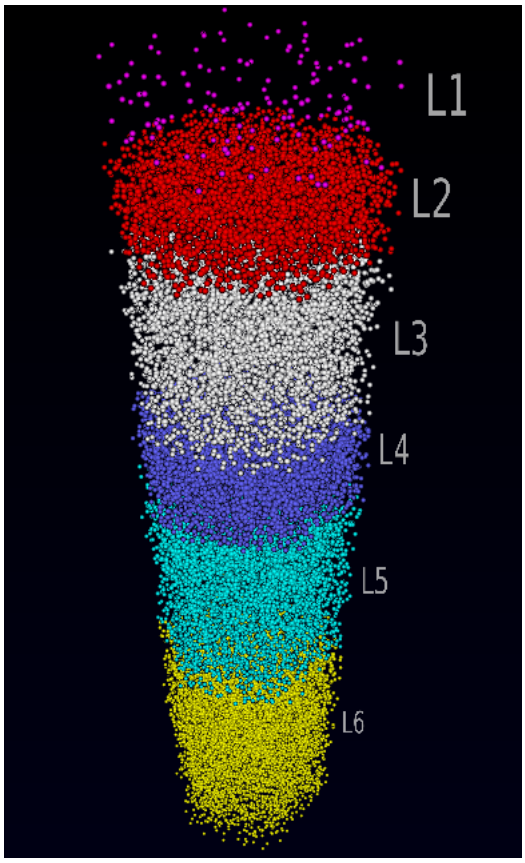

Figure 3: Visualization in 3D of the cortical point-neuron column used for the detailed simulation. Different layers of the column are color-coded for a better overview.

Parameter	Excitatory type	Inhibitory type	Description
C_m	73.05 pF	73.05 pF	Membrane capacitance
a	−5.165 nS	−0.9896 nS	Subthreshold adaptation
b	111.8 nA	8.862 nA	Spike-triggered adaptation
V_T	−52.0 mV	−57.0 mV	Spike threshold
Δ_T	2.0 mV	2.0 mV	Slope factor
g_L	8.594 nS	7.349 nS	Leak conductance
E_L	−74.35 mV	−70.92 mV	Leak reversal potential
τ_w	55.27 mV	1000.0 mV	Adaptation time constant
t_{ref}	5.0 ms	5.0 ms	Refractory time
V_{peak}	−30.0 mV	−30.0 mV	Peak voltage
E_{exc}	0.0 mV	0.0 mV	Excitatory reversal potential
E_{inh}	−70.0 mV	−70.0 mV	Inhibitory reversal potential

Table 2: Adaptive exponential integrate-and-fire model equation parameters for both types of neurons and their values used for the point-neurons in the detailed simulation.

The synaptic input current was computed according to equation-5, with the normalized time-dependent synaptic conductivity defined as an exponential decay function with time constant $\tau_{syn,e/i}$.

$$g_{norm}(t) = exp\left(\frac{-t}{\tau_{syn,e/i}}\right) \tag{13}$$

$\tau_{syn,e/i}$ had a different value for either excitatory or inhibitory synapses, these values being

$$\begin{aligned} \tau_{syn,e} &= 0.2ms \\ \tau_{syn,i} &= 2.0ms \end{aligned}$$

One can notice that since all neurons of the same type (excitatory or inhibitory) have the same AdEx model constants, and therefore behave in the same way in terms of potential evolution, this simulation did not take in account some of the morphological differences between neurons, other than those due to a different synaptic connectivity. The point-neurons were therefore morphologically distinguished according to their pre- and post-synapses, instead of their behavioral characteristics.

3.1.2 Computational aspects

In order to simulate the column activity, the NEST software ([19]) was used. It offered to parallelize the calculation on different processor cores, resulting in a time-efficient simulation. NEST also avoided the creation of a weight matrix, which would have resulted in Memory problems, because of the $31000 * 31000 * 8$ bytes $\approx$ 7.7Gb datasize for each synaptic parameter and variable, in double precision floating point numbers.

Even with a parallelization of the task on 8 processor cores, the ratio between the total simulation time and simulated column activity time was in the order of $T_{tot}/T_{sim} \approx 100$ on an 8 core Intel i7 960 3.20Ghz processor, with a simulation timestep of $dt = 0.1ms$. This was not only due to the high number of neurons and the much higher number of synapses, but also to the complexity of the used model which took in account the whole timecourse of the neuron potentials, as opposed to the mean-field model simulation studied later in this project, which computed directly the firing rate of the neurons.

The results were plotted using the matplotlib library for python ([18]).

To have a better overview of the activity propagation between different layers, a 3-dimensional visualization of the column was also implemented, using the compiled C++ langage with the OpenGL ([21]) and SDL ([23]) libraries. The neurons of the column had spherical representations and were placed at their biological positions.

3.1.3 Simulation Results

Column neurons in-vivo have a non-zero firing rate (spontaneous activity) which is caused by activity arriving from the surrounding network. To mimic this external activity, we applied a constant external input to all neurons of the column (Brunel N. (2000)). This resulted in a non-zero firing rate, called base rate in this report. By doing so, any change from the base rate of the layer 4 neurons will result in a rate change in the targeted layers, even if very low.

In order to account for the biological layer 4 input, an additional external current was used in form of a step current, to study its propagation in the column layers (see figure-4).

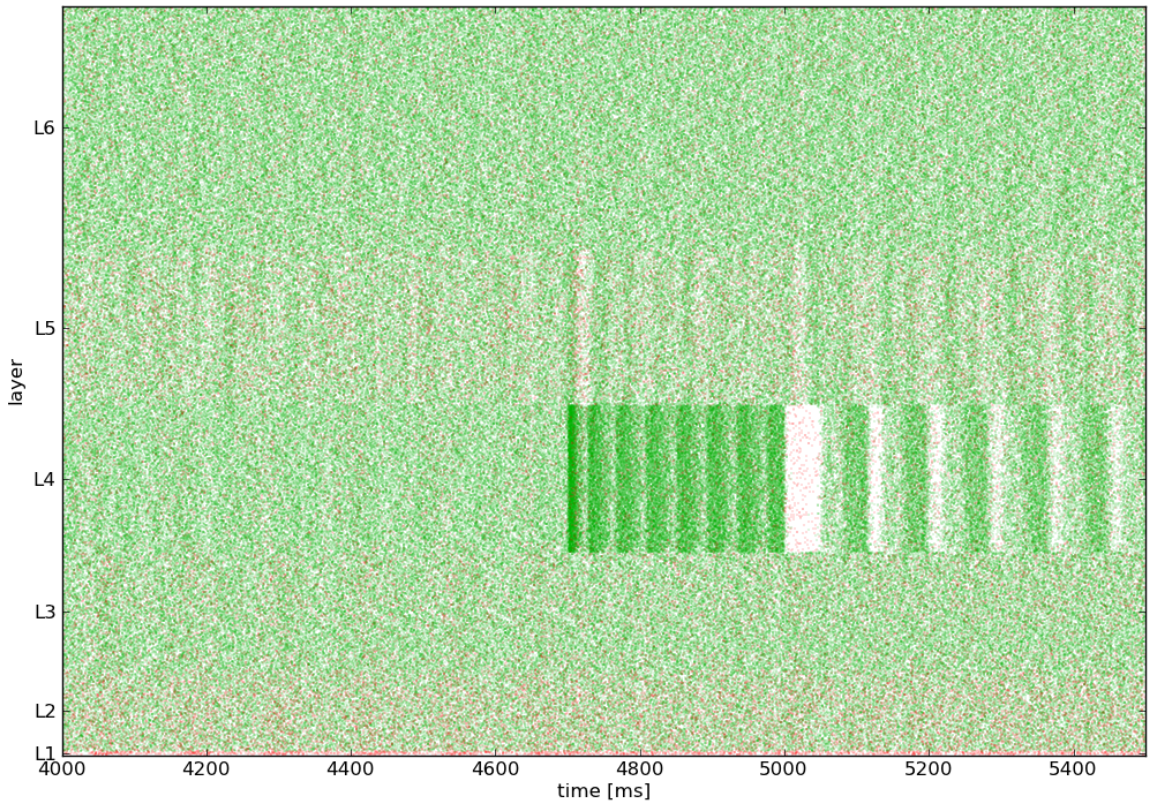

Figure 4: Spike raster plot of the cortical column data containing 31000 neurons, for a constant input for each neuron of $I^{ext} = 200pA$ and an external step current into population L4e at time $4700ms < t < 5000ms$ of $I^{add}_{L4e} = 200pA$. Spikes of excitatory and inhibitory neurons are distinguished by color (respectively *green* and *red*) and their layer of origin is indicated on the y-axis.

Layer 4 responds with a synchronous activation of all cells during the current step. This response is followed by a long supression of activity as the stimulus is switched off, as well as reverberations of the firing rate which persist until the end of the simulation. This is a particular characteristic of the AdEx neuron model, and is created by the adaptation variable w that has an offset at every firing spike of the neuron. For a high firing rate, this can led to an increased value of w which then needs a certain time period to go back to its original value. This feature of the same firing rates could not be reproduced using the mean-field model populations, as it was not taking in account any neuron refractoriness or adaptation.

There is also, a weak response of layer 5, the biological output layer of the column. It is however much weaker than expected ($dF_{max} = 0.2Hz$), and information propagation is almost negligible (see figure-5). The firing rate evolution was measured as a convolution of the firing spikes with the alpha function defined as

$$\alpha(t) = t \cdot e^{-t/\tau_\alpha}$$

with $\tau_\alpha = 100ms$ which was long enough to reflect the validity range of the mean-field model, while getting a smooth rate evolution.

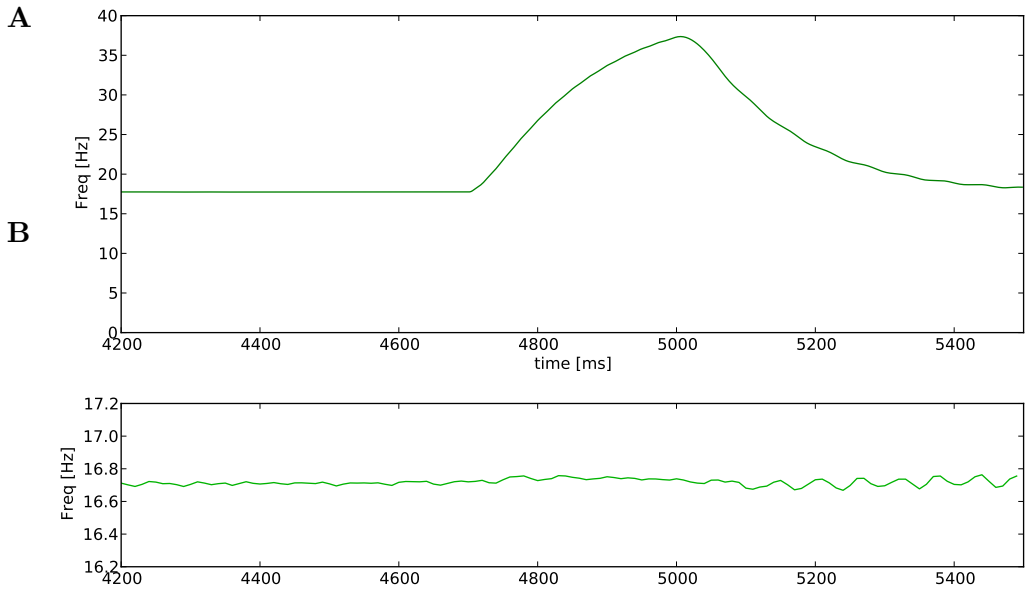

Figure 5: Firing rate timecourse of (**A**) L4e and (**B**) L5e populations, for a constant input for each neuron of $I^{ext} = 200pA$ and an external step current into population L4e at time $4700ms < t < 5000ms$ of $I^{add}_{L4e} = 200pA$.
The y axis scale of the L5e rate evolution has been scaled to improve readability.

3.2 Mean-field model populations

The second simulation consisted of applying the mean-field model equations to a certain number of populations, to be able to reproduce the same long-term behavior and activity propagation as in the cortical column.

3.2.1 From voltage based to current based model

In the mean-field model originally described by Tsodyks M., Pawelzik K. and Markram H., the external input I^{ext} and the weights of the connections J in equation-12 are respectively in units of Volt (mV) and voltage-per-frequency (mV/Hz). This difference was preventing any comparison between the mean-field and the AdEx model in terms of behavior, since the external input for the AdEx model could only be given in units of current (pA).

A way to avoid this problem was to change both the external input and the connection weights from voltage based into current based units. For the dimensions of the model agree, the activation function $h(I)$ also had to be changed to give the response rate of a population to a given input current. Fortunately, this could be done in a rather straightforward way, since the activation function was not defined in a precise way by the mean-field model itself, but rather by the neurons of the population that was simulated.

3.2.2 Population parameters

The mean-field equations 7 and 12 were implemented to simulate any number of populations. The parameters and variables of the simulation and their dimensions are summarized in table-3.

Variable	Dimensions	Units (SI)	Description
F	N	Hz	Population firing rate
x	N^2	-	Fraction of available resources
U_{SE}	N^2	-	Fraction of resources used at spike
Parameter	**Dimensions**	**Units (SI)**	**Description**
N	1	-	Number of populations
τ_m	N	s	Membrane time constant
τ_{rec}	N^2	s	Recovery time constant
τ_{fac}	N^2	s	Facilitating time constant
U^0_{SE}	N^2	-	Step increase of fraction of resources used U_{SE}
J	N^2	A/Hz	Connection Weight
I^{ext}	N	A	External input

Table 3: Parameters and variables of the mean-field model simulation and their dimension, unit and description.

Since the variables x and U_{SE} are different for each synapse, their dimension was N^2. As a result, the number of computations at every timestep increased with N^2, if all populations were connected together. The number of synaptic parameters τ_{rec}, τ_{fac}, U_0 and J also followed the number of synapses, and left a high number of dimensions in parameter space.

The activation function $h(I_{tot})$ of the mean-field model (see equation-12) was defined by a linear threshold function:

$$h(I_{tot}) = \begin{cases} 0 & \text{if} \quad I_{tot} < \theta \\ \beta(I_{tot} - \theta) & \text{if} \quad I_{tot} > \theta \end{cases} \tag{14}$$

θ being the threshold of the neuron, and β being the increase of firing rate after the threshold is reached. I_{tot} was the total input current of a neuron.

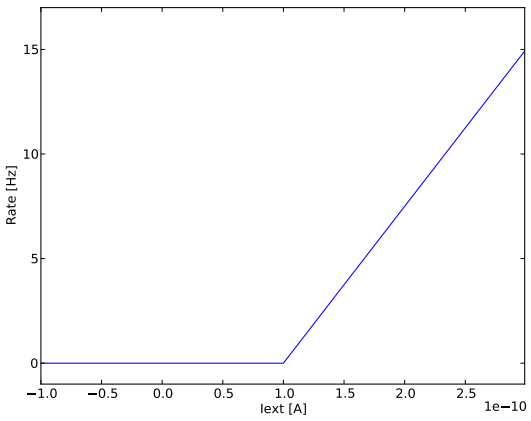

Figure 6: Activation function used in the first part of the mean-field model simulation, with $\theta = 100pA$ and $\beta = 0.075Hz/pA$.

From section-4.1 on, this linear function is replaced by a more plausible transfer function, which we determine by measuring the rate transfer function of an AdEx model neuron.

3.2.3 Computational aspects

The simulation of N mean-field populations was implemented in the interpreted language Python, using the libraries Numpy ([20]) and Scipy ([22]). These offered advanced yet simple access to mathematical manipulations and with good performance. Therefore, even thought

the complexity of the algorithm was $\mathcal{O}(N^2)$, the Numpy library allowed an efficient solution of the mean-field model equations.

For the mean-field equations, the 3 variables F (rate), x (available resources) and U (synaptic efficacy) must be computed at every timestep. We started by using the classic Euler algorithm, because it is simple and stable. In terms of performance and precision however, the Euler algorithm did not offer satisfactory results, as it required a very low simulation timestep to reach adequate accuracy. For a better accuracy, the 4-th order Runge-Kutta algorithm was implemented, which reduced the total simulation time by an order of magnitude while increasing precision. The code of the implementation of the Euler algorithm is shown in appendix-1, and for the Runge-Kutta 4 algorithm in appendix-2.

3.2.4 Simulation Results for a Single Population

To validate the mean-field model and to explore its basic behavior, we simulated one population of excitatory neurons with an autaptic connection. Even in such a simple system, predicting the steady-state firing rate of the population was non-trivial because of the depression and facilitation of the connection.

Figure-7 shows two simulations of a population with a strong depressing connection. In figure-7A, the steady-state firing rate is reached after a long oscillatory transient. Figure-7B illustrates that for different parameters and initial condition the rate relaxes to its steady-state value after a strong excursion. This shows that for a slightly different excitatory connection weight, the evolution of the firing-rate and its steady-state value can quickly change.

A facilitating synapse will in most cases result in an unstable network activity, because the increasing synaptic efficacy U_{SE} leads to an increase of the population rate, which in turn increases the synaptic efficacy even more. This is illustrated in figure-8.

Such high firing rates are biologically impossible, since actual neurons have a certain refractory time after each spike during which they cannot fire. The current activation function $h(I_{tot})$ is linear and not limited for $I_{tot} > \theta$, therefore

$$\lim_{I_{tot} \to +\infty} h(I_{tot}) = +\infty$$

whereas a more realistic activation function would be such that

$$\lim_{I_{tot} \to +\infty} h'(I_{tot}) < \frac{1}{t_{ref}}$$

This was later solved in section-4.1, by introducing a new activation function that was computed numerically from the AdEx neuron model and had therefore an upper limit, while also possessing a biological non-linearity.

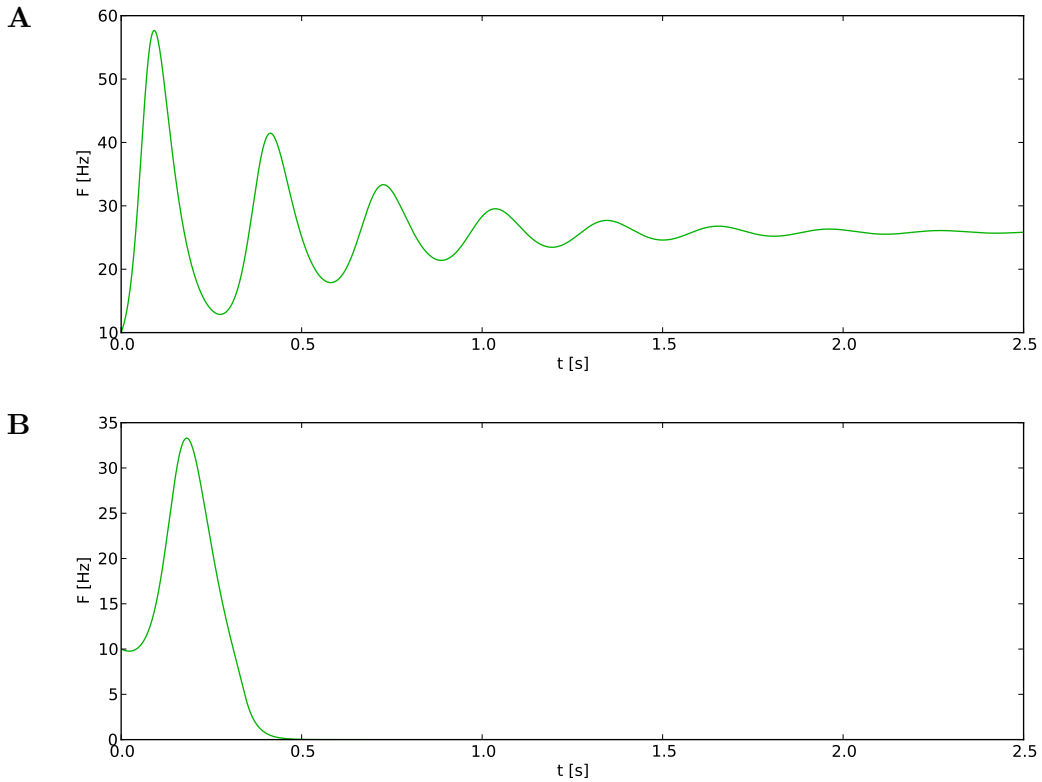

Figure 7: Rate timecourse of a single excitatory mean-field population with a depressing autaptic connection.
(**A**) Paramaters of the connection are $\theta = 100pA$; $\beta = 0.075Hz/pA$; $U^0_{SE} = 0.5$; $\tau_{rec} = 800ms$; $\tau_{fac} = 5ms$; $J = 390pA/Hz$.
(**B**) Parameters as in A, but with $J = 300pA/Hz$.

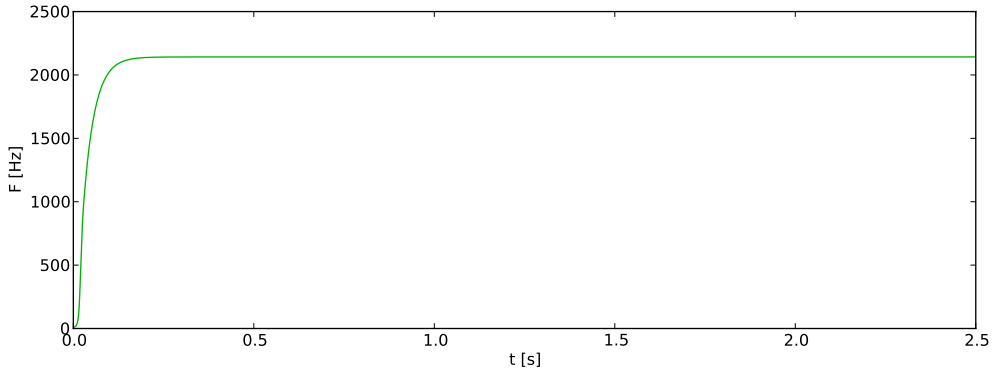

Figure 8: Rate timecourse of single excitatory population with a mostly facilitating autaptic connection.
Paramaters of the connection are $\theta = 100pA$; $\beta = 0.075Hz/pA$; $U^0_{SE} = 0.5$; $\tau_{rec} = 10ms$; $\tau_{fac} = 500ms$; $\tau_m = 30ms$; $J = 300pA/Hz$. The firing rate of the population quickly reaches extremely high values and remains only stable because of the slight depression of the connection.

3.2.5 Simulation results for 2 populations

Next we investigated the rate evolution of two populations, one excitatory and one inhibitory. The two populations had autaptic connections to themselves, and also to the other population. The system had therefore a total of four connections. The parameters used in this section are listed in table-4.

Activation function parameters	$\theta = 100pA$	$\beta = 0.075Hz/pA$
External input	$I_e^{ext} = 113.3pA$	$I_i^{ext} = 100.0pA$
Membrane time constant	$\tau_{m,e} = 30ms$	$\tau_{m,i} = 30ms$
Synaptic efficacy increase	$U^0_{SE,ee} = 0.5$ $U^0_{SE,ie} = 0.05$	$U^0_{SE,ei} = 0.5$ $U^0_{SE,ii} = 0.03$
Recovery time constant	$\tau_{rec,ee} = 800ms$ $\tau_{rec,ie} = 600ms$	$\tau_{rec,ei} = 800ms$ $\tau_{rec,ii} = 850ms$
Facilitating time constant	$\tau_{fac,ee} = 0.5ms$ $\tau_{fac,ie} = 1000ms$	$\tau_{fac,ei} = 0.5ms$ $\tau_{fac,ii} = 400ms$
Connection weights	$J_{ee} = 333pA/Hz$ $J_{ie} = 466pA/Hz$	$J_{ei} = -266pA/Hz$ $J_{ii} = -131pA/Hz$

Table 4: Model parameters and their values used for the simulation of an excitatory and an inhibitory mean-field population, connected together.

As seen in figures-9A, B and C, there was a large set of solutions to the mean-field model equations applied to a system of only 2 populations coupled together, only by changing one variable of the system (J_{ee}). The rates followed very different regimes such as a periodic one (see figure-9A), an irregular one (see figure-9B) and another one that reached steady-state after a few oscillations (see figure-9C).

The number of different regimes can even be higher, given the multitude of different synaptic and neuronal parameters used, and an entire analysis of such a high dimensional system could hardly be done numerically.

Next we computed the response of 2 populations to an external input. A current step of $I^{add} = 300.0pA$ was applied in the time range $1000ms < t < 1500ms$ to the excitatory (figure-10A) and inhibitory (figure-10B) population. The figures show not only the rate change of the targeted populations in response to the current step, but also the propagation of the activity into the other population. One can notice the absence of a propagation delay, since this is neglected by the mean-field model used.

Notice that the response of the excitatory population (figure-10A) is followed by a deep rate suppression and a dampened oscillation, resembling the response pattern of the excitatory point-neurons shown in figure-(4).

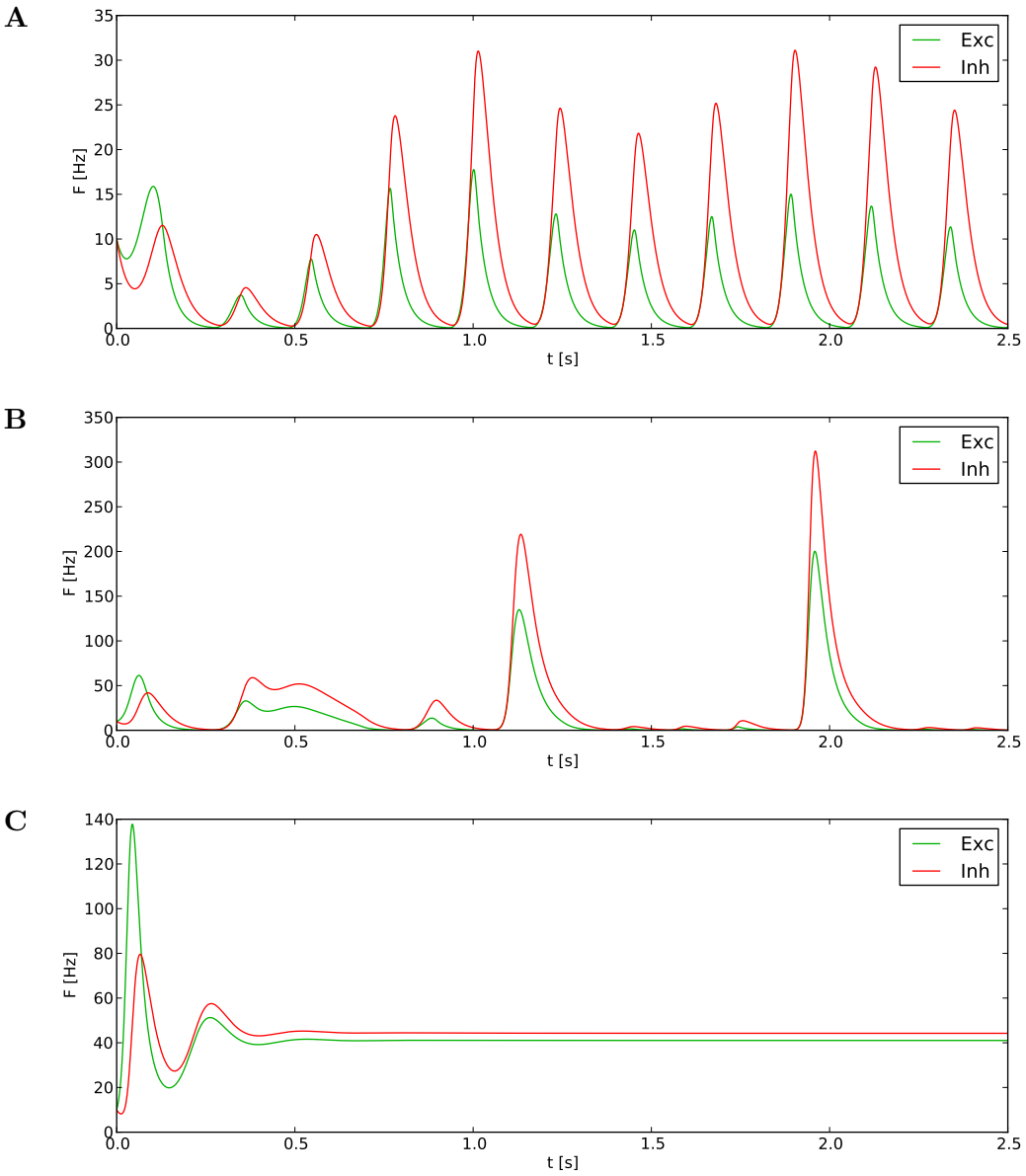

Figure 9: Rate timecourse of an excitatory and an inhibitory population mutually connected and having autaptic connections.
(**A**) Parameters of the connection are listed in table-4.
(**B**) Parameters are the same as in A but with $J_{ee} = 490pA/Hz$.
(**C**) Parameters are the same as in A but with $J_{ee} = 720pA/Hz$.

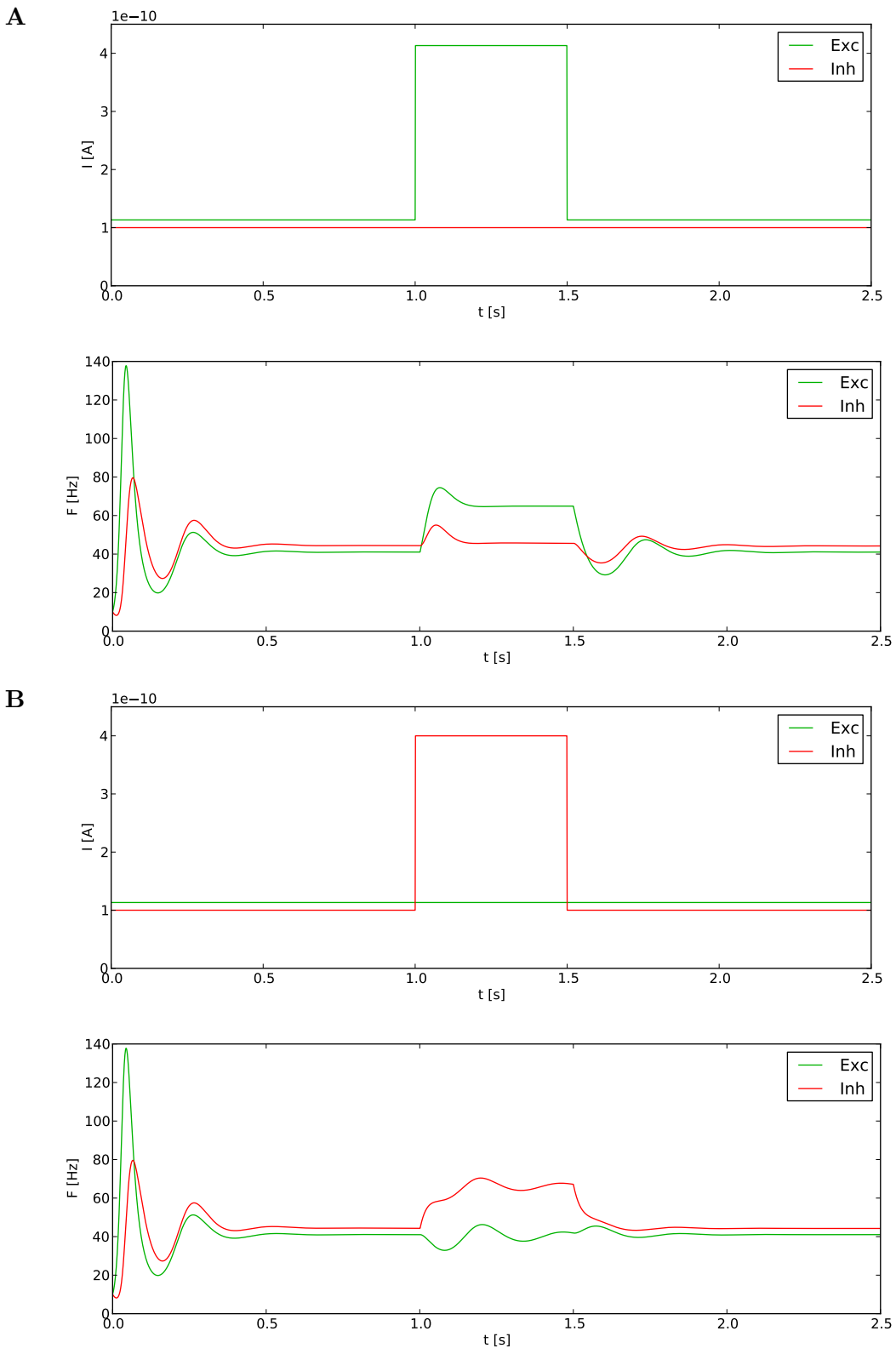

Figure 10: Rate timecourse of an excitatory and an inhibitory population connected together and having autaptic connections. Parameters of the connection are listed in table-4 but with $J_{ee} = 720pA/Hz$. In addition to the external input, a step current of $I^{add} = 300.0pA$ in the range $1000ms < t < 1500ms$ was applied to (**A**) the excitatory and (**B**) the inhibitory population.

4 Parameter calibration for 55 mean-field model populations

Each synapse of the cortical column has a set of parameters and contributes to the diversity of interactions between neurons. One of the most challenging parts of the reduction of the whole column into a few populations was, thus, to be able to eliminate some of this diversity while keeping a similar global behavior.

Since the connectivity of the column and the characteristics of the different synapses are mainly determined by the type of the pre- and post-synaptic neurons and their layer of origin, the most straightforward way to divide the column into a certain number of populations was by distinguishing them by type and layer. This biologically driven approach led to a total of 55 populations accross the column, that were then simulated using the mean-field equations. The number of neurons in every of these 55 populations is shown in figure-11.

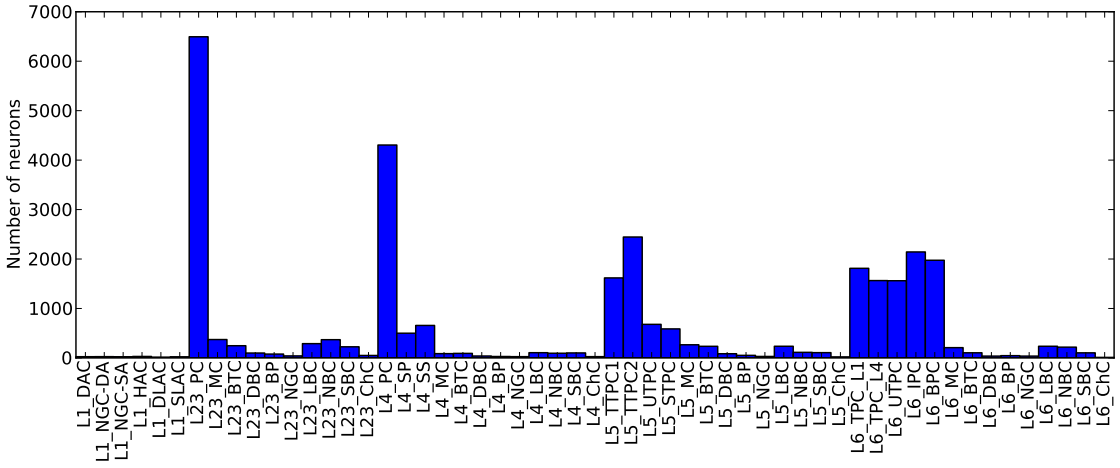

Figure 11: Number of neurons per population for the 55 morphologically and layer-wise distributed populations.

For these populations to emulate the long term behavior of the point-neuron column, it was vital to compute their different mean-field parameters by using the column data. Such parameters were the activation function $h(I_{tot})$ and the connection constants such as the connection weight J.

This section will first focus on obtaining the correct activation function $h(I_{tot})$ to match the rate response of a mean-field population for a given input current, to that of an AdEx point-neuron. Then, the different connection weights J will be calculated to go from a spike-based synaptic input to a rate based one. Finally, the remaining synaptic parameters will be retrieved from the column, to incorporate them into the mean-field network.

The synaptic time delays were not taken in account in the mean-field connections, because of their value in the order of at most a few milliseconds. The study was focused around much longer-term behavior.

4.1 Activation function calibration

As described in section-3.2, the activation function $h(I_{tot})$ was artificially defined to make the neuron population rate linearly increase for inputs higher than the threshold (equation-14). Althought being a good approach to mimic the activity of a neural population, this did not allow to reproduce the behavior of a complicated neural system such as the cortical column, because the AdEx model has a non-linear I-F curve. Althought the rate response of a neuron

can often be approximated by an analytical function (Shriki O., Hansel D., Sompolinsky H. (2003)), it was not possible here.

Rather, we estimated the activation function of an AdEx neuron numerically, by computing its firing rate response to a constant input current. Althought this function was only valid for the steady-state rate of the neuron, it was sufficient to reproduce the long-term behavior of the column.

The two types of neurons distinguished in the detailed simulation were the excitatory and inhibitory types. There were therefore only 2 different activation functions to be computed. For the full BBP column, one would need to estimate the I-F curve for each neuron type.

In order to numerically obtain the two different activation functions needed, a constant external input was applied to a single AdEx neuron of excitatory or inhibitory type. By iterating this experiment over a large number of values of the external input and computing the steady-state response rate of the neuron, the activation function could be measured (see figure-12).

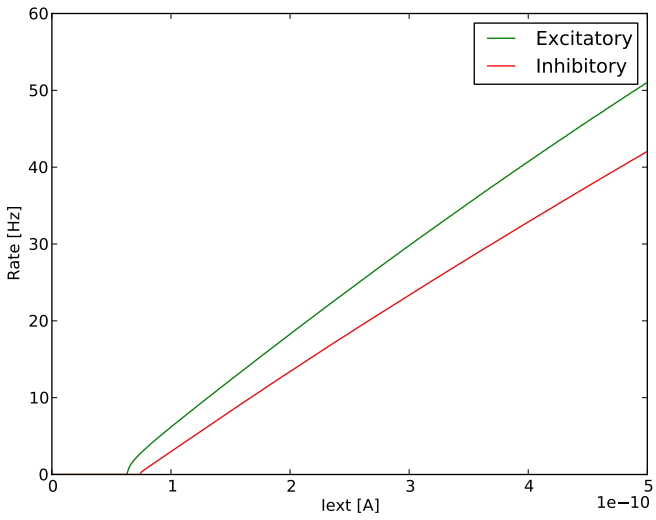

Figure 12: Activation function of the excitatory and inhibitory AdEx neurons used in the detailed point-neuron simulation of the column.

For the following simulations, we used these functions in the evaluation of the mean-field equations-14. As the rate values of this function were only computed for a finite number of different external inputs, a linear interpolation was applied to get the response rate of a neural population to any external input.

The validation of the obtained activity function was done by giving a constant input $I^{ext} = 200pA$ to a population of 100 point-neurons without any connections and to a corresponding mean-field population, for both excitatory and inhibitory types. Apart from the transients at the start and the end of the simulus, which cannot be captured by the mean-field model, the rate evolutions of the 2 methods showed a good agreement and thus confirmed the usage of the computed activation function (see figure-13).

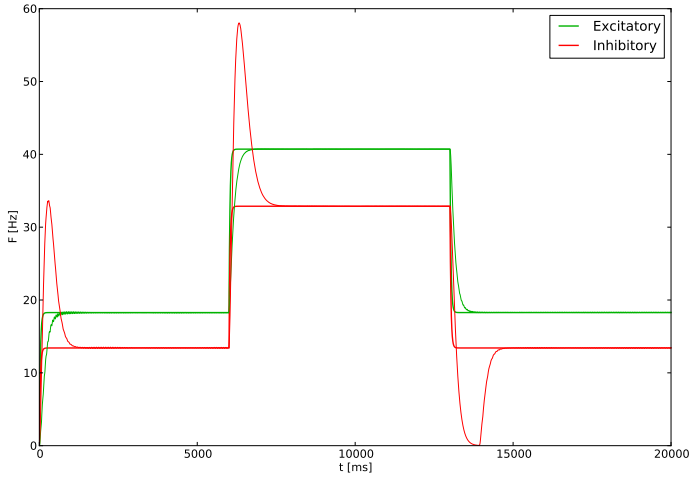

Figure 13: Rate evolution of a point-neuron population of 100 neurons (*thin line*) and of its corresponding mean-field model population (*broad line*), for both excitatory and inhibitory type. The populations have a constant external input current of $I^{ext} = 200pA$ with an additional current step at time $6000ms < t < 13000ms$ of $I^{add} = 200pA$.

One can observe that short-term behaviors such as the response of the point-neuron population to a current step, is not captured by the activation function, and therefore cannot be reproduced by the mean-field model. This is however not problematic in the context of this project, since only the long-term rates of the cortical column have to be approximated.

4.2 Mean-field model weight computation from the AdEx model

As seen in section-2.2 in the column point-neuron simulation (equations 5 and 13), the synaptic current induced by a presynaptic spike at time $t = 0$, that flows into the postsynaptic neuron can then be written as

$$I(t) = U_{SE} \cdot x \cdot \bar{g} \cdot exp\left(\frac{-t}{\tau_{syn,e/i}}\right) \cdot (E_{e/i} - V)$$

The synaptic input current into an AdEx point-neuron depends strongly on the potential of the neuron at any time. Unfortunately, this cannot be translated in a straightforward way into a mean-field model weight, since mean-field populations do not possess any potential, but rather a firing rate. The task is to get from a dynamic current input that depends on the post-synaptic neuron potential, to a static connection weight.

When studying the evolution of the potential of a periodically firing neuron, one can notice that its average value in time is very similar for different firing rates (see figure-14). One can observe that its value is almost constant in the range of frequencies higher than $5Hz$ (see figure-15). This is confirmed by the fact that its derivative over the rate is very low ($|\frac{d\bar{V}}{dF}| < 0.2mV/Hz$) in that same range of frequencies for both types of neurons (see figure-16).

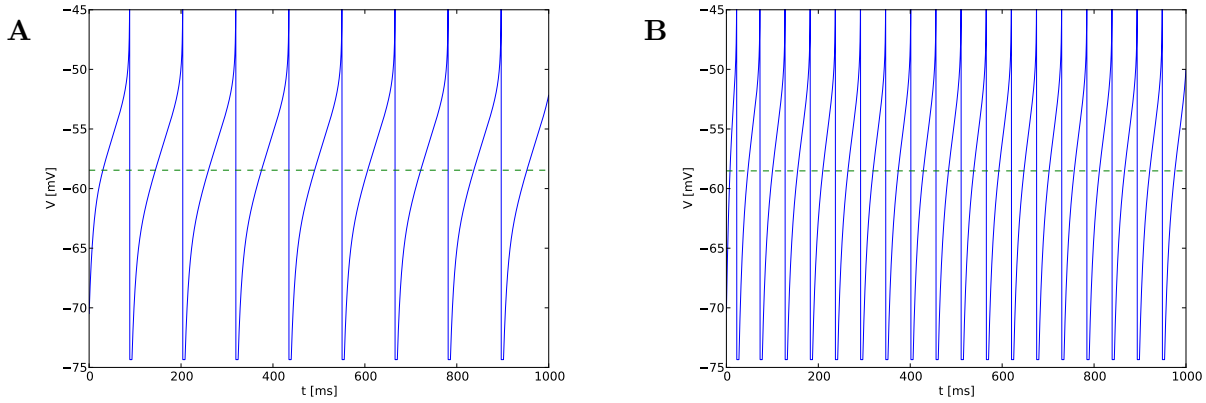

Figure 14: Timecourse of an excitatory AdEx neuron potential (*full line*) and it average value (*dashed line*) for an external input current of (**A**) $I^{ext} = 120pA$ and (**B**) $I^{ext} = 200pA$.
We observe that the mean value of the membrane potential is similar for both frequencies.

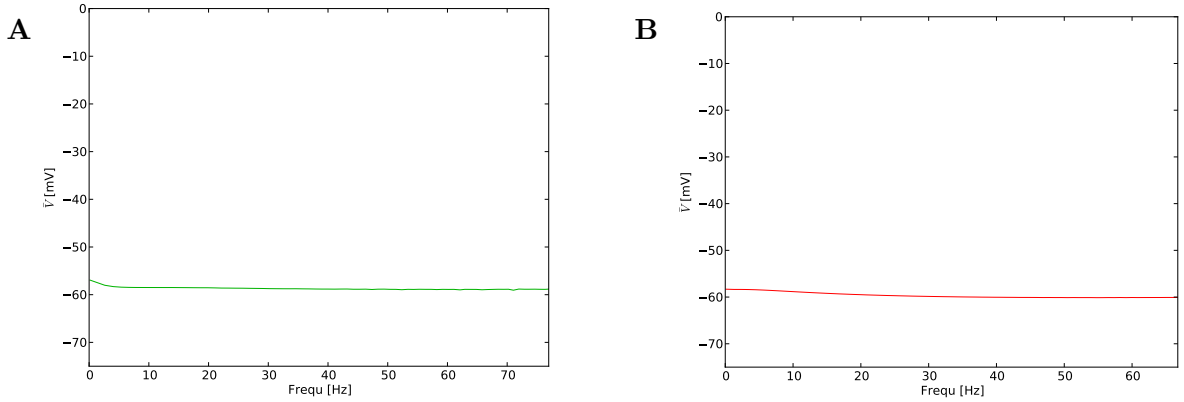

Figure 15: Average potential for different firing rates of (**A**) an excitatory and (**B**) an inhibitory AdEx neuron, which stays almost constant for most frequencies.

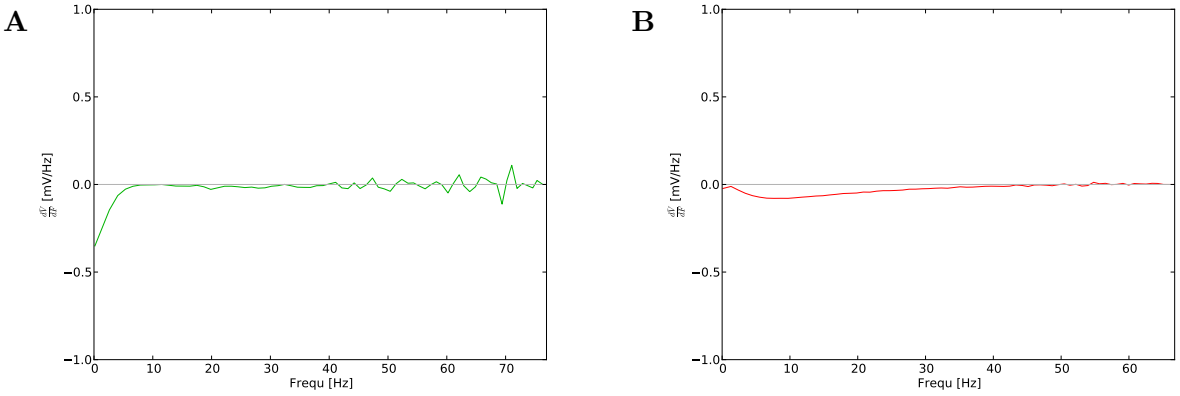

Figure 16: Derivative of the average potential over the rate, according to the rate, for (**A**) an excitatory and (**B**) an inhibitory AdEx neuron, which exhibits very low values, confirming the low change in the mean potential.

Because such a small change in the given range of frequencies, the average potential $\bar{V}$ can be taken as a constant. Its value for a neuron firing in the range of 5-65Hz was therefore taken to be

$$\begin{aligned} \bar{V}_E = &\quad -58.735mV \\ \bar{V}_I = &\quad -59.680mV \end{aligned}$$

for the excitatory and inhibitory post-synaptic neuron type, respectively.

The calculation of the arithmetic mean of the potential can be justified, since the resulting current depends linearly on the potential, ie. $I(t) \propto (E_{e/i} - V)$.

Assuming an average potential $\bar{V}$ for a repetitively firing neuron and using the expression for the synaptic input current (equation-5), the total amount of charges that flows into a cell at every synaptic spike in case of a static synapse, can be written as

$$\begin{aligned} Q_{tot} &= \int_0^\infty I(t) \cdot dt \\ &= \bar{g} \cdot (E_{e/i} - \bar{V}) \cdot \int_0^\infty exp\left(\frac{-t}{\tau_{syn,e/i}}\right) \cdot dt \\ &= \bar{g} \cdot (E_{e/i} - \bar{V}) \cdot \tau_{syn,e/i} \end{aligned} \tag{15}$$

This calculation was done by assuming that the post-synaptic neuron voltage stayed constant during the synaptic current flow. This is the case if the exponential current decay is short and the input current is low, preventing the potential from undergoing a great change during the current decay.

The total synaptic current entering a repetitively firing pre-synaptic neuron is $Q_{tot} \cdot F_{pre}(t)$. Since the total connection input current of a mean-field population is by definition the quantity $U_{SE} \cdot x \cdot J \cdot F_{pre}(t)$, it is possible to use the previous expression of the input charge to write

$$\begin{aligned} U_{SE} \cdot x \cdot J \cdot F(t) &= U_{SE} \cdot x \cdot Q_{tot} \cdot F(t) \cdot M_{sy}/N_{post} \\ &= U_{SE} \cdot x \cdot \bar{g} \cdot (E_{e/i} - \bar{V}) \cdot \tau_{syn,e/i} \cdot F(t) \cdot M_{sy}/N_{post} \end{aligned} \tag{16}$$

where the right-hand side of the equation was multiplied by $U_{SE} \cdot x$ for a dynamic synapse. Also, as we are interested in the total current entering the population, the right-hand side was also multiplied by the number of synapses M_{sy} arriving at said population. In order to get the average input current of the population cells, one also has to scale the total current by the number of neurons N_{post}. $\bar{g}$ is the maximal conductance averaged over all synapses between the pre- and post-synaptic populations.

It is then possible to isolate J as

$$J = \bar{g} \cdot (E_{e/i} - \bar{V}) \cdot \tau_{syn,e/i} \cdot M_{sy}/N_{post} \tag{17}$$

which is now a constant and can be used for the mean-field simulation.

4.3 Synapse parameters calibration

The last parameters needed by the mean-field model were the recovery time constant τ_{rec}, the facilitating time constant τ_{fac}, and the synaptic efficacy increase per spike U_{SE}^0 (see table-3). Since the extended Tsodyks-Markram synapses in the point-neuron column used the same parameters as the mean-field model, retrieving these synaptic parameters seemed straightforward. However, instead of having multiple synapses going from a pre- to a post-synaptic neural population each with different synaptic constants, the mean-field connections have only one set of such constants (see figure-17).

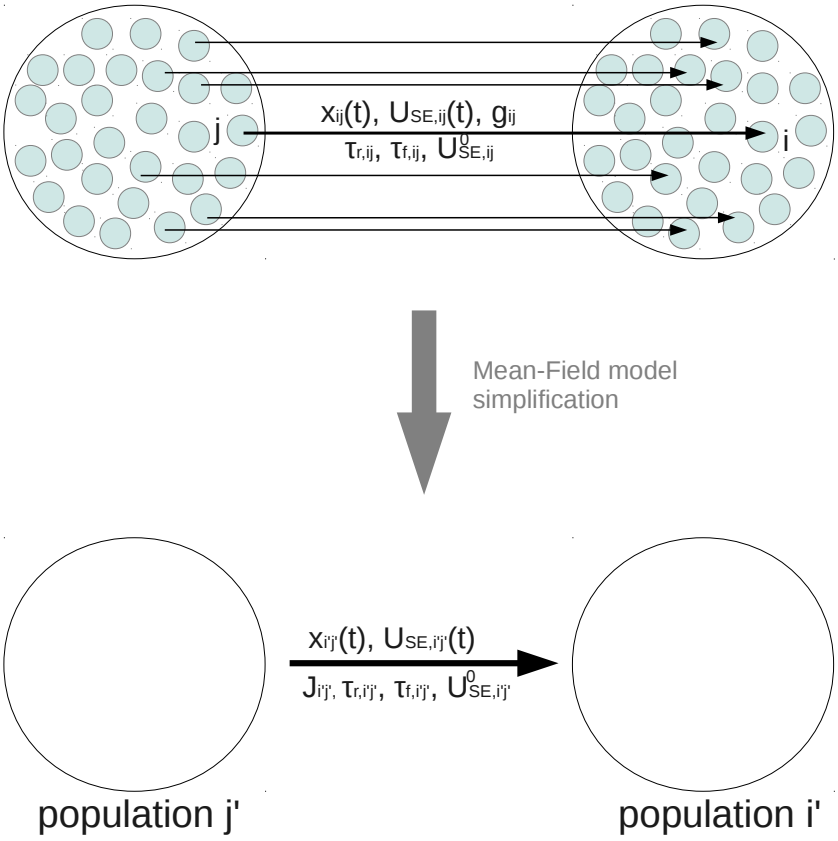

Figure 17: Reduction of the synapses between 2 mean-field populations to a single connection, with averaged synaptic parameters.

Therefore, all synaptic constants of a given connection had to be combined and their arithmetic mean was taken for the resulting mean-field connection (see figure-18 as an example for the recovery time constant distribution in one connection). While this may seem the most straightforward approach, it is only valid if the distribution of the given parameters was narrow, ie. had a low standard-deviation. The reason for this is that none of these parameters had a linear effect on the system, and the mean-field equations were too complex to allow for an analytical formula of a correctly weighted averaging. The consequences of this approximation are studied in section-5.3.

The different parameter mean values are shown in figures 20, 21, 22 and 23 for 55 mean-field populations and illustrate the diversity of the column in terms of synaptic parameters.

One can notice the absence of synapses between certain populations, even if the two populations are spatially close to each other in the column (see figure-19). The chandelier cells (ChC) for example of any layer only have outgoing synapses to excitatory populations, and never to inhibitory ones. This shows that the connectivity between populations is strongly determined by their type. This also justifies the separation of neurons into several populations by their type.

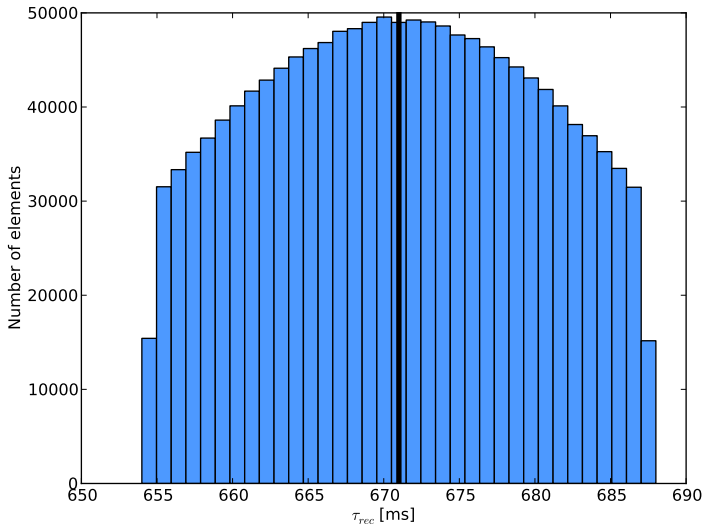

Figure 18: Distribution of the recovery time constant τ_{rec} values of the autaptic synapses of population $L5_{TTPC2}$. The arithmetic mean of the distribution that is used for the mean-field model connections, is also shown.

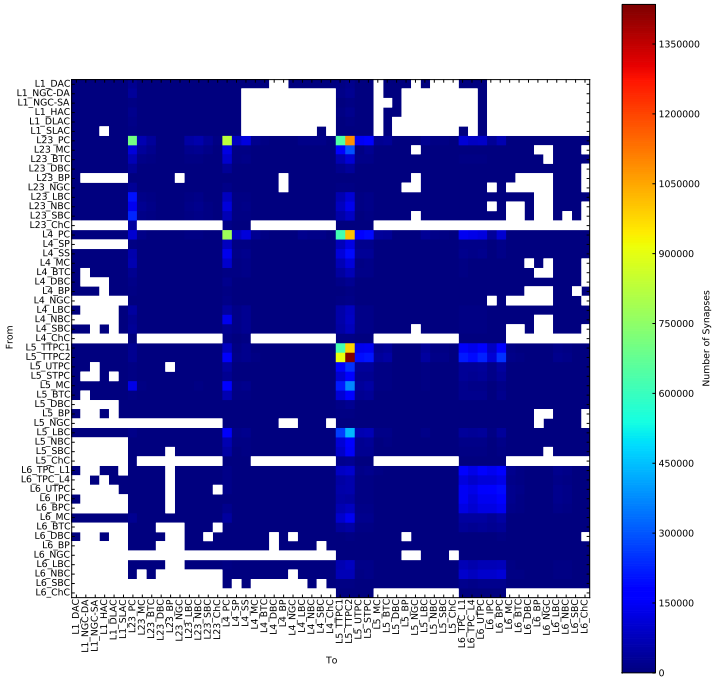

Figure 19: Number of synapses between the 55 different populations.

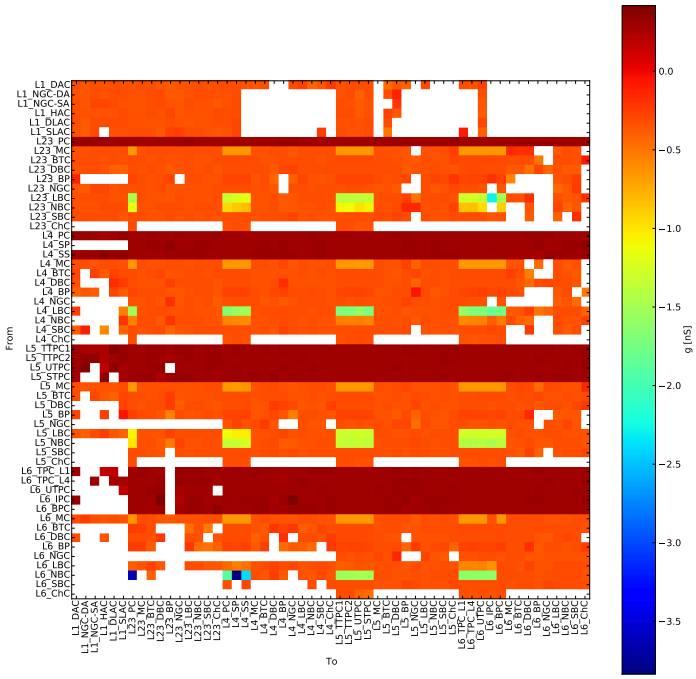

Figure 20: Average synaptic conductance between the 55 different populations. Negative conductance values stand for inhibitory synapses.

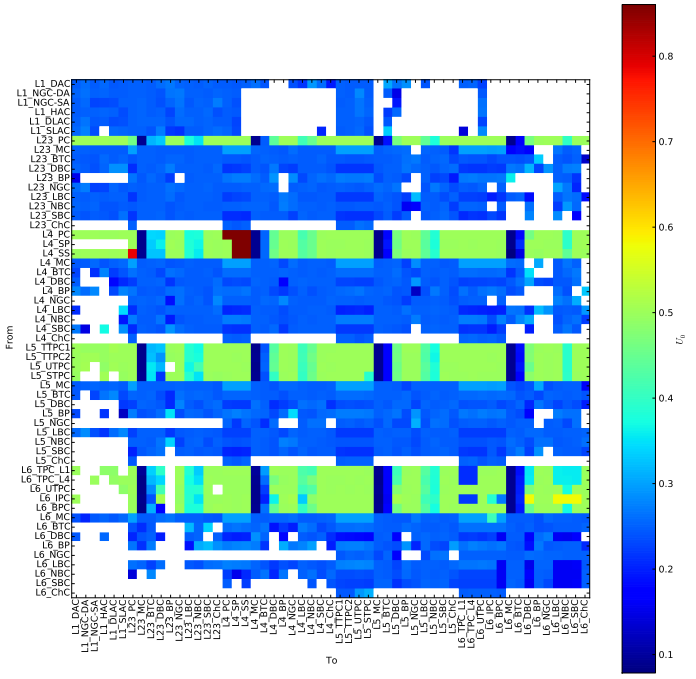

Figure 21: Average synaptic efficacy increase between the 55 different populations.

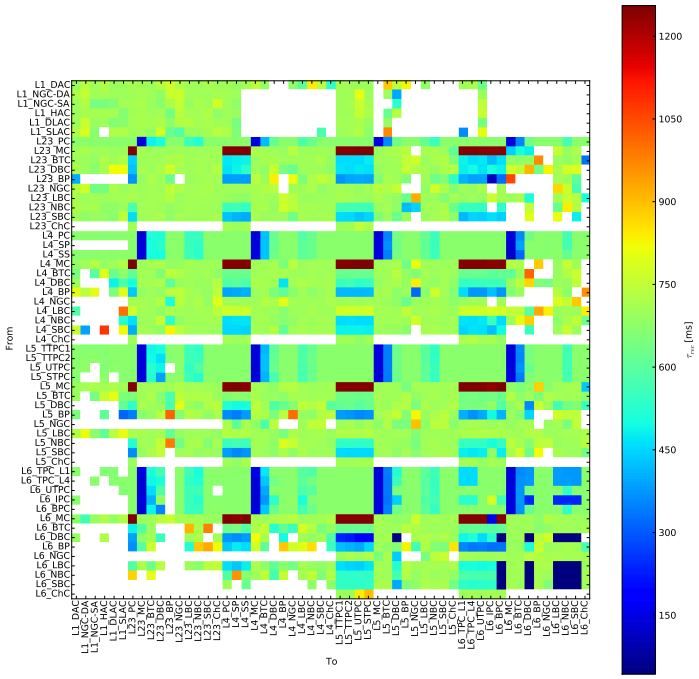

Figure 22: Average synaptic recovery time constant between the 55 different populations.

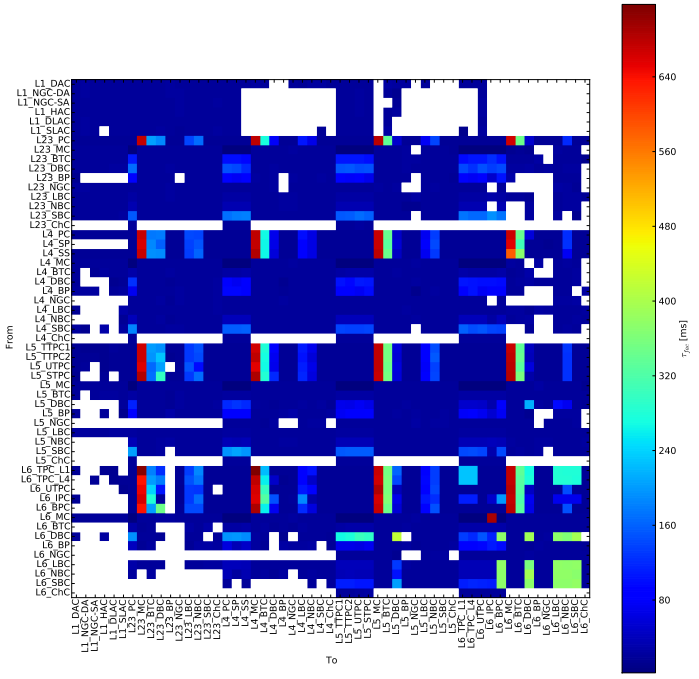

Figure 23: Average synaptic facilitating time constant between the 55 different populations.

5 Sources of errors

5.1 Correlation error

The derivation of the mean-field model for the dynamic synapses described in section-2.4 assumed that the two variables x and U_{SE} are independent. So the first source of errors in the mean-field model results from the correlation between x and U_{SE}. Althought the relative error between $\langle xU_{SE}\rangle$ and $\langle x\rangle\langle U_{SE}\rangle$ should never be higher than 10%, besides for high values of U^0_{SE} and low values of τ_{fac} (Tsodyks M., Pawelzik K. and Markram H.), this could sometimes be the case in the column (for example $U^0_{SE} > 0.8$ and $\tau_{fac} < 30ms$). This resulted in a systematic and inavoidable error in the mean-field simulations.

5.2 Averaging errors of the population model

Another source of error was the approximation of the weights J_{ij} between the different populations. This was done by setting the potential of a repetitively firing neuron to an average value $\bar{V}$. While this assumption was true for neurons receiving a constant input current, it was not always the case for synaptic inputs. Since synaptic input currents strongly depend on the membrane potential, a continuously spiking presynaptic neuron can modify the potential distribution $P(V)$ of the postsynaptic cell, leading to a different average potential.

For example in case of an inhibitory synapse, the post-synaptic cell receives a much weaker inhibition when its potential is low and therefore close to the reversal potential, and a much stronger inhibition when its potential is high and thus further away from the reversal potential. As a consequence, the neuron will spend more time having a high potential value as it would have been in case of a constant external inhibitory current with the same average amplitude (see figure-24). This effect is also present in case of excitatory inputs, althought much less significant since the neuron potential is much further away from the excitatory reversal potential.

The approximation of the average potential $\bar{V}$ to a constant value can therefore only be true for weak synaptic inputs. This is however not always the case in the column simulation, and the use of corrected values $\bar{V}^{corr}$ is required to take in account this effect. Unfortunately, even when these values are measured directly in the column during a simulation with constant input, they would still be different from one simulation to the other, depending on the column activity.

This error does unfortunately not have any trivial approximation, as the AdEx equations are not solvable analytically, and the synaptic current is not constant during the simulation.

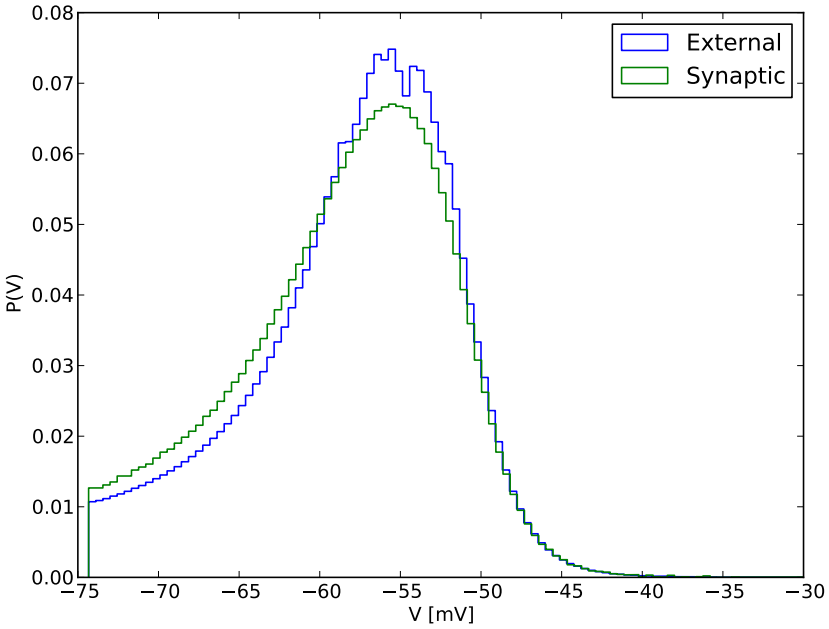

Figure 24: Potential distribution $P(V)$ of an excitatory AdEx neuron that receives a constant external input current of $I^{ext} = 200pA$. It is also receiving input from wether an inhibitory neuron with synaptic conductance $g = 5.0nS$ and a poissonian firing rate of $\nu = 100Hz$, or a constant external input current of the same average amplitude.

5.3 Averaging errors of the synaptic parameters

Another source of errors results from averaging the synaptic constants between populations. Since the data was taken from biological measurements, every synapse in the column had different synaptic constants. By simplifying a certain number of synapses to a single mean-field model connection, the synaptic diversity was taken away.

The resulting problem is that the different synaptic constants were not linearly additive, and the approximation of using the arithmetic mean only works if the standard-deviation of the respective constant is low. The actual values for the standard-deviations between the 55 populations are shown in appendix-4.

To test the magnitude of this error, the steady-state values for a constant external input of $I^{ext} = 200pA$ to every cell of the column were compared for the simulation with the original column, and the same simulation but with all synaptic constants set to their average values. This eliminated the standard-deviation of those synaptic constants. The connection constants were averaged between 55 morphologically chosen populations of the column, resulting in a 55×55 sized matrix for all the parameter values.

Table-5 shows the errors on the firing rates, as well as the deviations from the base rates. The relative error of a steady-state firing rate F' compared to another one F is defined as

$$E_{tot} = \left| \frac{F - F'}{F} \right| \tag{18}$$

whereas its relative deviation error from the base rate is

$$E_{dev} = \left| \frac{(F - F_B) - (F' - F_B)}{F - F_B} \right| \tag{19}$$

with the base rate F_B being the steady-state rate of the population in case of no synaptic connections.

For some populations, the deviation error is as high as 65%, showing that the approximation of averaging over different synaptic constants has already a significant impact on the simulation results. Since this error solely results from removing the parameter diversity, it will be present in even the most faithful mean-field model.

The relative error on the total rates of the populations is very low. This is the case because the weights in the column are so low, that the deviation of the population rates from their base rate is very small compared to their actual values.

Population name	Base rate [Hz]	Normal simulation rate [Hz]	Averaged synaptic constants ($\sigma_{syn} = 0$) simulation rate [Hz]	Total rate error E_{tot} [%]	Deviation rate error E_{dev} [%]
L1i	13.415	13.322	13.322	0.0	0.0
L23e	18.275	17.859	17.856	0.0152	0.6531
L23i	13.415	13.330	13.343	0.0949	14.89
L4e	18.275	17.749	17.706	0.2431	8.202
L4i	13.415	13.506	13.551	0.3326	49.36
L5e	18.275	16.728	16.457	1.6221	17.54
L5i	13.415	13.663	13.763	0.7336	40.42
L6e	18.275	18.029	17.939	0.4973	36.44
L6i	13.415	13.530	13.605	0.5565	65.48

Table 5: Steady-state rates of the different column populations for an external input $I^{ext} = 200pA$, for the point-neuron simulation of the original column and that of a modified version in which all synaptic parameters between populations had been set to their average value ($\sigma_{syn} = 0$).

6 Behavior comparison between the 2 models

In order to compare the behavior of the point-neuron and the mean-field models, their steady-state firing rates were measured for a constant external input of $I^{ext} = 200pA$ into all populations. For clarity's sake, the rates of the 55 populations were eventually merged into 9 rates (L1i, L23e, L23i, L4e, L4i, L5e, L5i, L6e and L6i), by calculating their weighted mean according their neuron count.

The mean potentials $\bar{V}$ for excitatory and inhibitory neuron types are measured in the column during the simulation, which gave much better results than the original values calculated previously. The corrected values for the mean potentials were thus set to $\bar{V}_e^{corr} = -57.030mV$ and $\bar{V}_i^{corr} = -59.004mV$, allowing the steady-state rates of the column to be approximated quite accurately, as long as the standard-deviation of the synaptic constants was eliminated (see figure-25A).

In this case, most of the mean-field rates converge to the steady-state rates of the point-neuron populations, with the noticeable exception of population $L5e$. The reason for the inaccuracy at predicting the rate of the latter is that it receives a much stronger synaptic inhibition than the other populations. This results in a higher average potential and therefore even the corrected potential values $\bar{V}_e^{corr}$ and $\bar{V}_i^{corr}$ cannot compensate this deviation.

The same mean-field rates are also compared to the steady-state rates of the non-modified column (see figure-25), with less accuracy due to the averaging of the synaptic constants.

The values of the steady-state rates are shown in Table-6, for the mean-field model simulation and both the normal point-neuron column simulation, and the modified point-neuron column with averaged synaptic paremeters ($\sigma_{syn} = 0$).

The relative error on the rates defined in equations 18 and 19 is computed (see Table-7), and shows a good precision of the mean-field simulation when compared to the modified version of

the column. The main source of error is due to the fact that some populations of the column get much stronger inputs than others, resulting in a change of their average potential value $\bar{V}$. As a consequence, the calculation of the mean-field connections loses much of its accuracy. Since the synaptic input of a neuron can change at any time of a simulation, a way to solve this would be to introduce a dynamic variable for the average potential, that would depend on the different synaptic inputs. The problem in doing so is not only that the AdEx model does not allow analytical calculations because of its complexity, but also that this approach would result in the creation of a different mean-field model, which is beyond the scope of this project.

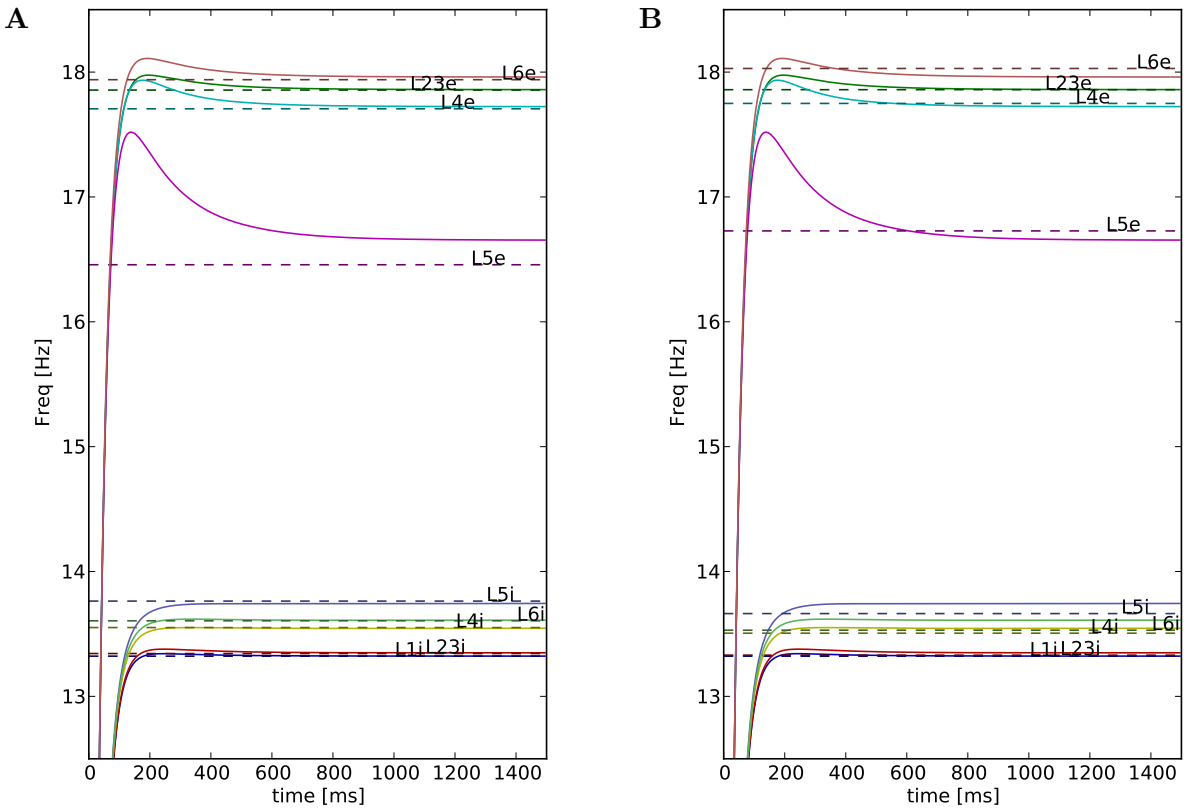

Figure 25: Comparison between rate evolution of the 55 mean-field populations with the adapted average potential values ($\bar{V}_e^{corr} = -57.037mV$ and $\bar{V}_i^{corr} = -59.004mV$) (*continuous lines*), and the column point-neuron simulation steady-state rates (*dashed lines*), for a constant current of $I^{ext} = 200pA$ applied to all populations. The column point-neuron simulation was done (**A**) without the standard-deviation of the synaptic constants (modified column) and (**B**) with the original column.

Population	Point-neuron column rate [Hz]	Point-neuron column averaged constants ($\sigma_{syn} = 0$) rate [Hz]	55 mean-field populations rate [Hz]
L1i	13.322	13.322	13.322
L23e	17.859	17.856	17.860
L23i	13.330	13.343	13.349
L4e	17.749	17.706	17.724
L4i	13.506	13.551	13.545
L5e	16.728	16.457	16.654
L5i	13.663	13.763	13.744
L6e	18.029	17.939	17.960
L6i	13.530	13.605	13.610

Table 6: Steady-state rates of the different column populations for an external input $I^{ext} = 200pA$, for the 55 population mean-field model simulation and both normal and modified column ($\sigma_{syn} = 0$) point-neuron simulations.

Population	Modified column ($\sigma_{syn} = 0$)		Normal column	
	Total rate error E_{tot} (%)	Rate deviation error E_{dev} (%)	Total rate error E_{tot} (%)	Rate deviation error E_{dev} (%)
L1i	0.002	0.336	0.002	0.336
L23e	0.020	0.866	0.004	0.151
L23i	0.043	8.109	0.141	22.162
L4e	0.099	3.098	0.143	4.823
L4i	0.042	4.213	0.291	43.154
L5e	1.200	10.863	0.439	4.751
L5i	0.138	5.440	0.593	32.688
L6e	0.121	6.438	0.379	27.792
L6i	0.040	2.842	0.594	69.913

Table 7: Relative error on the steady-state rates of the different column populations for an external input $I^{ext} = 200pA$, between the 55 population mean-field model simulation and both normal and modified column ($\sigma_{syn} = 0$) point-neuron simulations.

7 Further reduction of the column to 13 populations

The synapses between the 55 populations of the mean-field column can be simplified to 6 different categories, these being depressing, facilitating, or pseudo-linear, for both excitatory and inhibitory types (Ramaswamy et al. (2012)). Since the populations were determined due to their connectivities in the column, all cell types having a similar connectivity according to these synapse categories, could be merged. This led to a simplification from the original 55 populations to only 13 populations. The resulting populations and their neuron count can be seen in figure-26.

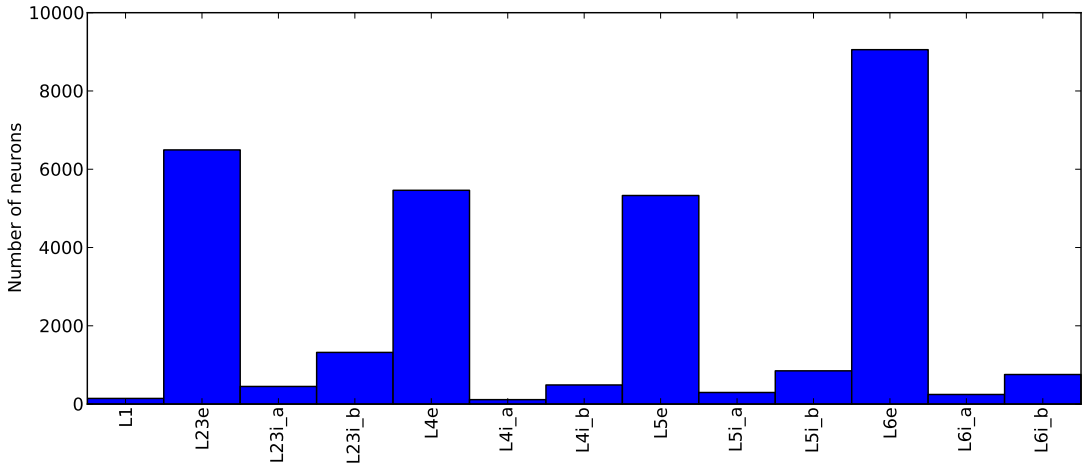

Figure 26: Number of neurons per population for 13 populations.

The synaptic parameters had to be retrieved and averaged again for the 13 mean-field populations, as shown in figures 27, 28 and 29.

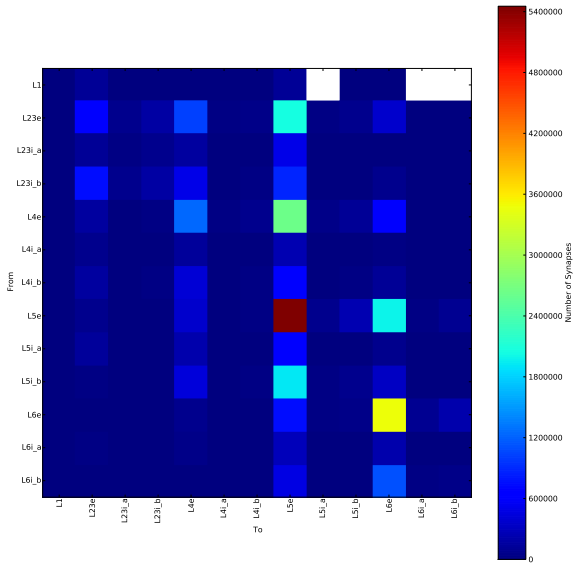

Figure 27: Number of synapses between the 13 different populations.

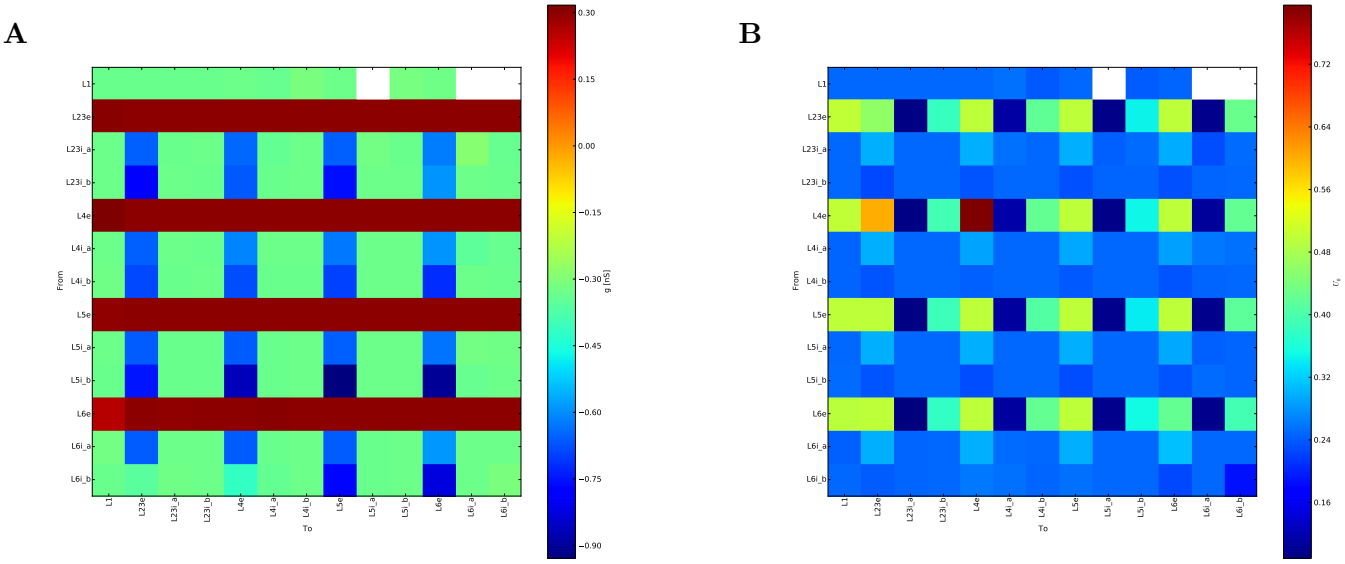

Figure 28: Average (**A**) synaptic conductance and (**B**) synaptic efficacy increase between the 13 different populations. Negative conductance values stand for inhibitory synapses.

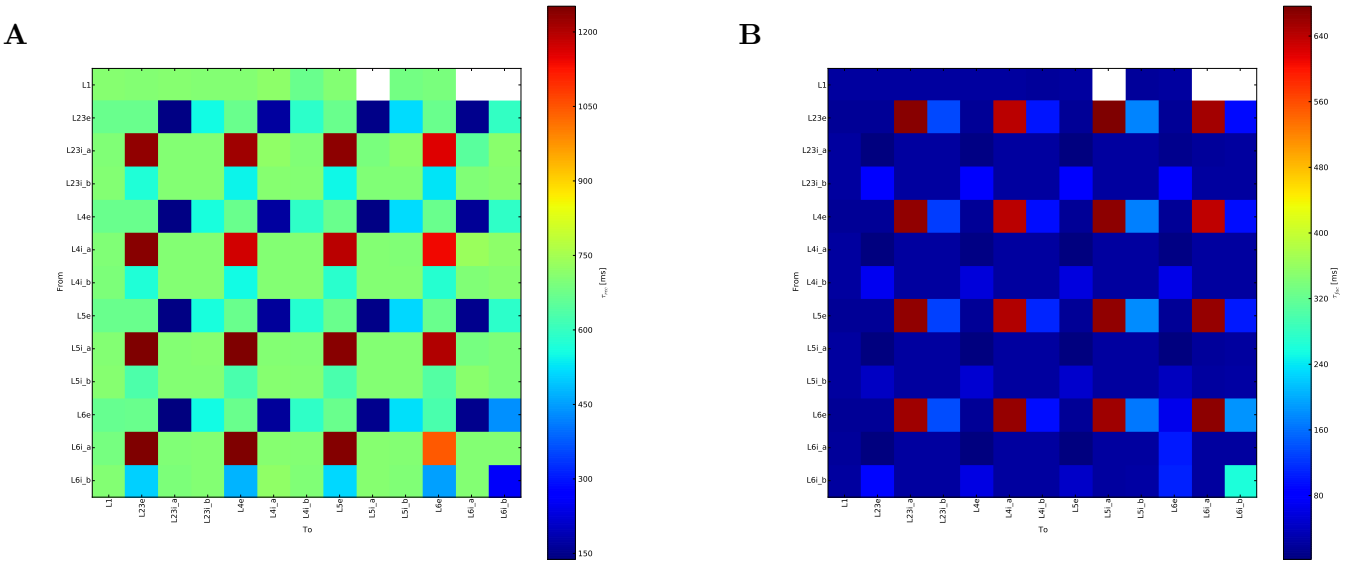

Figure 29: Average synaptic (**A**) recovery time constant and (**B**) facilitating time constant between the 13 different populations.

As for the 55 mean-field populations, the steady-state rates were again compared to the column populations, and the 13 mean-field populations, merged into 9 final populations for better clarity on the final rates. This reduction to a small number of populations led to an overall higher relative error on the steady-state rates, such as over 28% for population L5e on

the deviation from base rate, when compared to the simulation of the modified column with averaged synaptic constants (see figure-30A and Table-8).

The error defined in equations 18 and 19, was even higher when compared to the actual column simulation, because of the initial averaging on the connection constants. This error was even higher as it was for the 55 populations, because of the greater loss of information about the synapses when reducing the connectivity to a 13×13 matrix. The relative deviation error on the firing rate could therefore go up to over 100% in the worst case (see figure-30B and Table-9).

However, the error was in most other cases in the same range of values as for 55 populations, showing that despite such a drastic reduction of the number of parameters, the 13 mean-field populations can still reproduce the column activity fairly well.

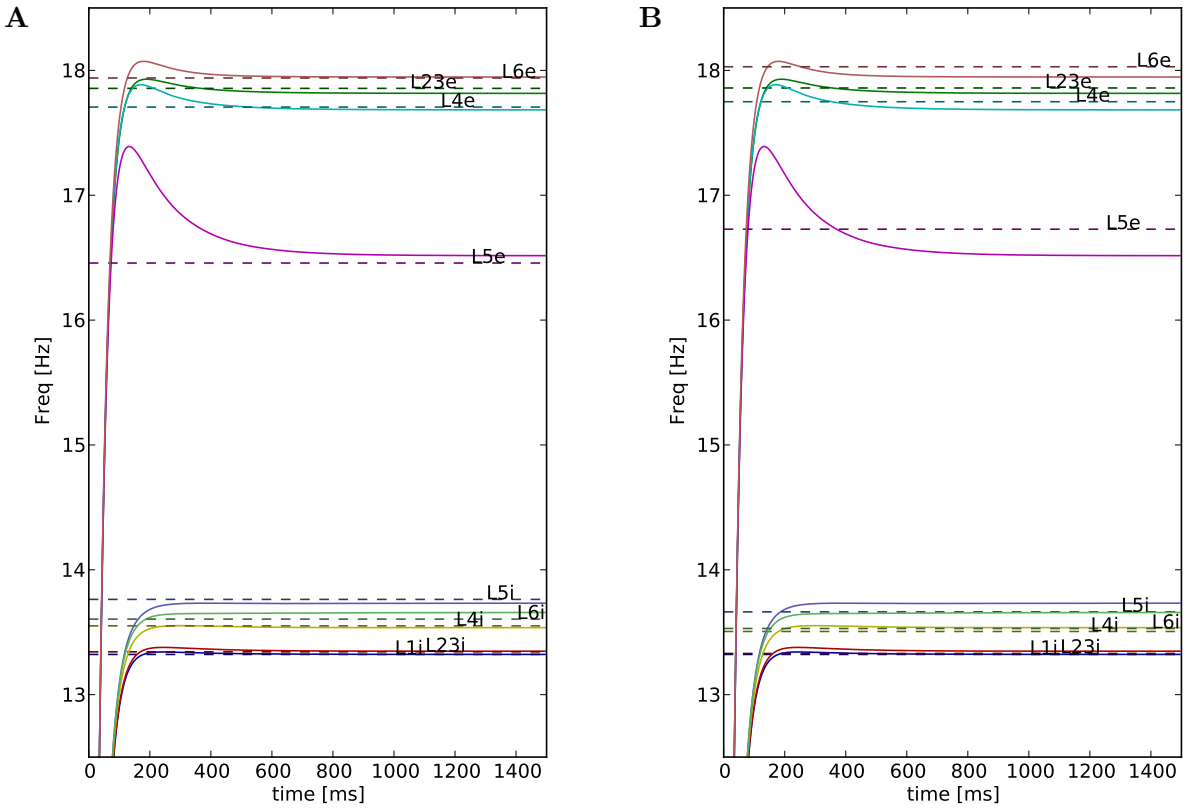

Figure 30: Comparison between rate evolution of the 13 mean-field populations with the adapted average potential values ($\bar{V}_e^{corr} = -57.037mV$ and $\bar{V}_i^{corr} = -59.004mV$) (*continuous lines*), and the column point-neuron simulation steady-state rates (*dashed lines*), for a constant current of $I^{ext} = 200pA$ applied to all populations. The column point-neuron simulation was done (**A**) without the standard-deviation of the synaptic constants (modified column) and (**B**) with the original column.

Population	Point-neuron column rate [Hz]	Point-neuron column averaged constants ($\sigma_{syn} = 0$) rate [Hz]	13 mean-field populations rate [Hz]
L1i	13.322	13.322	13.322
L23e	17.859	17.856	17.816
L23i	13.330	13.343	13.348
L4e	17.749	17.706	17.684
L4i	13.506	13.551	13.537
L5e	16.728	16.457	16.516
L5i	13.663	13.763	13.733
L6e	18.029	17.939	17.947
L6i	13.530	13.605	13.658

Table 8: Steady-state rates of the different column populations for an external input $I^{ext} = 200pA$, for the 13 population mean-field model simulation and both normal and modified column ($\sigma_{syn} = 0$) point-neuron simulations.

Population	Modified column ($\sigma_{syn} = 0$)		Normal column	
	Total rate error E_{tot} (%)	Rate deviation error E_{dev} (%)	Total rate error E_{tot} (%)	Rate deviation error E_{dev} (%)
L1i	0.003	0.405	0.003	0.406
L23e	0.224	9.565	0.241	10.356
L23i	0.038	7.073	0.136	21.286
L4e	0.125	3.894	0.367	12.388
L4i	0.106	10.548	0.227	33.686
L5e	0.358	3.243	1.268	13.707
L5i	0.220	8.723	0.510	28.083
L6e	0.044	2.327	0.456	33.407
L6i	0.388	27.832	0.945	111.200

Table 9: Relative error on the steady-state rates of the different column populations for an external input $I^{ext} = 200pA$, between the 13 population mean-field model simulation and both normal and modified column ($\sigma_{syn} = 0$) point-neuron simulations.

8 Synaptic plasticity

The main purpose of simplifying the column neurons to mean-field populations was to be able to reproduce its global behavior in terms of firing rate.

This should also allow to simplify a learning task, by applying it to the mean-field model populations, and then put back the modified weights into the column. The advantage of this method would be that the conductances of the high number of synapses ($\approx 3.5 \cdot 10^7$) would not have to be computed during the learning task, but only the connections between the mean-field population. This would result in a very high decrease in terms of computation time. On the other hand, the dimension of weights being drastically reduced, the mean-field populations might not learn certain tasks that require a high level of complexity of the network. Also, the number of inputs that go from the system into the network and the number of outputs that go back from the network to the system are limited by the number of populations used. The amount of information that the network can receive and send is greatly reduced, since the number of neurons decreased from the original 31000 to a few dozens.

The learning task studied in this section has therefore to be simple enough to allow the mean-field network to master it.

8.1 Introduction to the learning task

The learning task consisted balancing a ball placed in a circular arena, in order for it to reach the middle and stabilize. The arena was surrounded by a border in order to prevent the ball from falling down.

The arena was equipped with 5 receptive fields at given positions (see figure-31), that were activated when the ball was close to them. This provided the mean-field network with information about the position of the ball. The network could then change the inclination of arena, in response to the input.

Since the mean-field column has no spatial dimensions anymore, we had to re-introduce them by splitting each of the 13 populations in 5. One to represent the center of the arena and 4 surrounding it.

The synaptic parameters between the populations of the column had thus to be re-computed for $13 \times 5 = 65$ populations. In order to use a biological approach, the receptive field inputs were sent into the 5 populations $L4e$ as an external input current depending on the distance of the ball from each receptive field. In order for the receptive fields to cover the whole plate, the receptive fields were sending an external input current that was depending on the ball distance with a gaussian distribution. The input of the 5 receptor populations L4e was therefore

$$I^{ext}(t) = I_0 \cdot exp\left(-\frac{d^2(t)}{2\sigma^2}\right) \tag{20}$$

with d being the distance of the ball from the receptive field center, σ being the spacial standard-deviation of the receptive field, and I_0 maximal input current of the population.

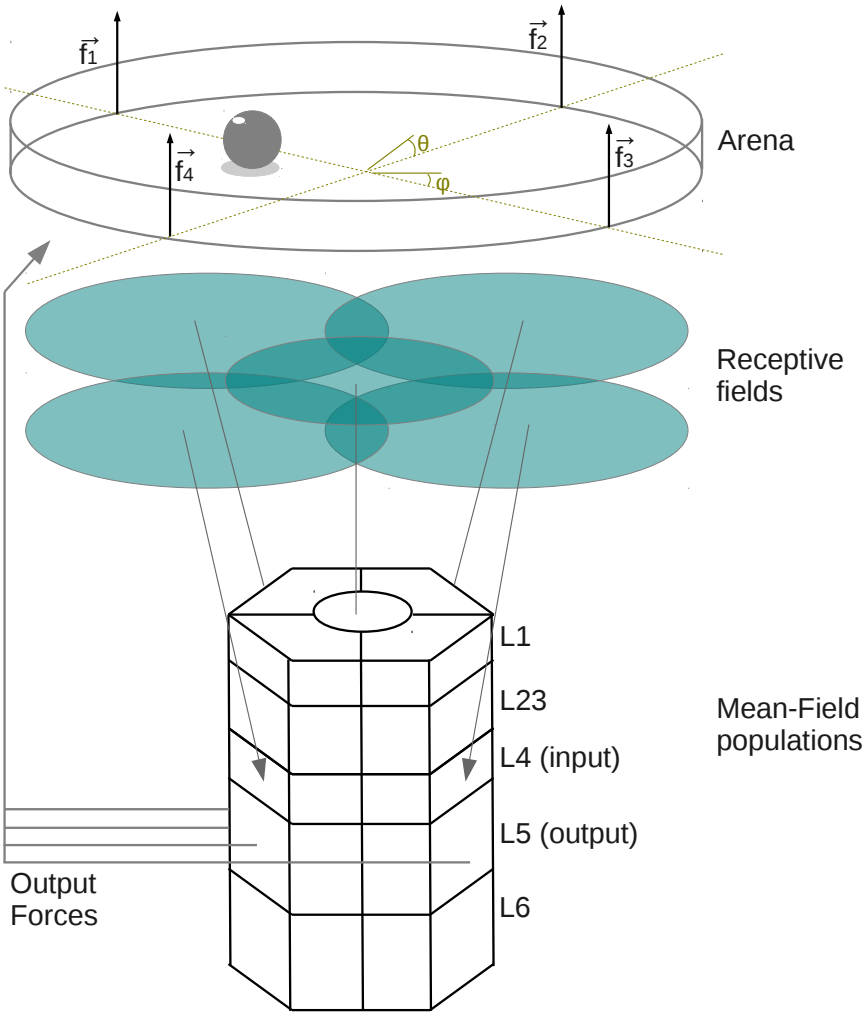

Figure 31: Ball balancing problem. Further division of the column neurons to 5×13 different populations had to be made in order for the network to detect the position of the ball on the plate.

The response of the network was taken from the 4 outer populations of L5e (the central population being excluded). The 2 targeted orientation angles of the plate were then changed proportional to the rate difference between the 2 opposing output populations, such that:

$$\begin{aligned} \phi_{targ}(t) &= S \cdot (F_{L5e\_1}(t) - F_{L5e\_3}(t)) \\ \theta_{targ}(t) &= S \cdot (F_{L5e\_4}(t) - F_{L5e\_2}(t)) \end{aligned} \tag{21}$$

with populations F_{L5e_1} and F_{L5e_2}, being respectively opposed to F_{L5e_3} and F_{L5e_4} on the plate. The scaling factor S, was a free parameter representing the physical response, such as muscle movement or force.

In order to dampen the short term effects that the system could have when the point-neuron column was being simulated instead of the mean-field network, the actual plate angles were set to converge to the targeted angle, with a time constant τ_{targ}, such as

$$\begin{aligned} \tau_{targ} \cdot \frac{d\phi(t)}{dt} &= \phi_{targ}(t) - \phi(t) \\ \tau_{targ} \cdot \frac{d\theta(t)}{dt} &= \theta_{targ}(t) - \theta(t) \end{aligned} \tag{22}$$

This also acted as a low-pass filter on the output system for a better stability of the plate. The reasoning behind setting the orientation of the plate to always approach a targeted angle, is for the physical system to have a certain delay before going to the orientation of destination set by the cortex.

The populations also received a constant external input current of $I^{ext} = 200pA$ to every population during the simulation, in order for them to posess a non-zero rate. The values of the different parameters are listed in Table-10.

8.2 Learning algorithm

In order to supervise the learning, a reward was given to the system, depending on the ball's position. The closer the ball was to the center of the plate, the higher was the reward. Its value was defined as

$$R(t) = R_0 \cdot exp\left(-\frac{d_C^2(t)}{2\sigma_R^2}\right) \tag{23}$$

with d_C the distance of the ball from the plate center, σ_R the spacial standard-deviation of the reward, and R_0 the maximal reward. The values of the static parameters are listed in table-10.

Name	Value	Description
σ	$0.05m$	Spacial standard-deviation of the receptive field
I_0	$300.0pA$	Maximal input current of the receptive field
S	$0.01rad/Hz$	Scaling factor for plate orientation
τ_{targ}	$10ms$	Time constant for actual plate angle to reach target angle
σ_R	$0.03m$	Spatial standard-deviation of the reward
R_0	1.0	Maximal value of the reward
r_{arena}	$0.1m$	Radius of arena
$d\eta$	$0.03pA/Hz^2$	Learning speed
r_{ball}	$0.004m$	Radius of ball

Table 10: Values and descriptions of the different constants of the plate balancing task.

In order to teach the mean-field network the task of ball balancing, a reward based Hebbian learning rule was used. The weight of the connection going from populations j to i in the network was updated at every timestep by

$$dJ_{i,j} = d\eta \cdot (R(t) - R(t - dt)) \cdot (F_i(t) - \bar{F}_i(t)) \cdot (F_j(t) - \bar{F}_j(t)) \tag{24}$$

$R(t)$ being the reward, $F_i(t)$ the rate of population i and $\bar{F}_i(t)$ the rate history of population i at time t. The latter was defined as the average of the rate $F_i(t)$, such as

$$\bar{F}_i(t) = \frac{1}{\Delta t} \cdot \int_{t-\Delta t}^{t} F_i(t) \cdot dt$$

with $\Delta t = 5.0s$. Furthermore, $d\eta$ was the learning step, that determined the learning speed and also the precision of the learning.

There were several reasons behind this learning rule. First, we would like to excule any learning rule that was just a supervised optimisation of the weights, rather than a biologically plausible learning. Second, the network with a hebbian learning rule without reward could not have learned the task, since it would not have had any information about the actual goal to achieve. Finally, the rate history $\bar{F}_i(t)$ of the populations was used, because even without the additional external inputs of the receptor populations in L4, every population had a base rate due to their constant external input. Therefore without the substraction of the rate histories from the current rates, every connection of the network would have been changed at every timestep, by following the sign of the reward change. Also, the change in reward is needed in the learning rule instead of only the value of the reward, so that the system *knows* if its last action contributed to achieve a better or a worst placement of the ball, than previously.

The learning procedure was thus the following:

1) Place the ball at a random position on the plate
2) Give an additional external input to one of the output populations to make the plate move
3) For each timestep:
   - Calculate reward according to $R(t) = R_0 \cdot exp\left(-\frac{d_C^2}{2\sigma_R^2}\right)$
   - Update weight at every timestep according to learning rule
     $dJ_{i,j} = d\eta \cdot (R(t) - R(t - dt)) \cdot (F_i(t) - \bar{F}_i(t)) \cdot (F_j(t) - \bar{F}_j(t))$
4) Repeat steps 1) to 3) every time period of $1s$ until task is learned for enough different positions of the ball

8.3 Computational aspects and mechanical properties of the system

The simulation of the mean-field model populations was done using the script previously described, since it could simulate any number of populations, given the parameters and the external input.

The 3D renderer and the physical interactions of the ball with the plate and with gravity were implemented in C++ using the OpenGL ([21]) and SDL ([23]) libraries. The position of the ball was updated using Euler algorithm for simplicity, such that

$$\begin{aligned} \ddot{\vec{x}}(t + dt) &= \vec{g} \\ \dot{\vec{x}}(t + dt) &= \dot{\vec{x}}(t) + dt \cdot \ddot{\vec{x}}(t + dt) \\ \vec{x}(t + dt) &= \vec{x}(t) + dt \cdot \dot{\vec{x}}(t + dt) \end{aligned}$$

dt being the time step of the simulation, $\vec{g}$ the gravitational acceleration, and $\ddot{\vec{x}}(t)$, $\dot{\vec{x}}(t)$ and $\vec{x}(t)$ respectively the acceleration, the velocity, and the position of the ball at time t. At every collision with the arena, the velocity of the ball was updated, using impulse responses, without any rotational term. The restitution coefficient of the balls speed was 0.4, and all other friction was neglected. The ball was therefore considered to be a punctual object, without any inertial value.

Since the physical interactions were computed in all dimensions of the space and the plate was actually rotated in response to network activity , the ball showed realistic physical behaviors such as bouncing on the arena when the rotational acceleration of the arena showed high values. This was done in contrast to previous models (Probst D. (2012)). The simplified impulse based equations for this system are described in appendix-3.

The Python script, calculating the rates of the mean-field model populations, and the C++ rendering and interaction program communicated with each other via local sockets. Therefore at every time step, the ball simulation sent an array with the position of the ball to the mean-field model computation, which calculated the external input of population L4e, and the response of the network. It then sent the rate of L5e output neurons back to the ball simulation.

This allowed an optimized simulation of both the mean-field populations, and the physical interactions. As a result, the bottleneck application of the simulation was usually the simulation of the mean-field model, since it was computationally much more expensive to solve, than the physical interactions of a ball and an arena.

8.4 Results

After sufficient learning time, the 65 mean-field populations were able to learn the task of plate balancing, by equilabrating the ball near the middle of the plate for any random initial position. An example of the ball trajectory is shown in figure-33A, and illustrates the efficiency of the network at accomplishing the task.

During different steps of the learning phase, a test was done in order to measure the ability of the network to accomplish the task. This was done by placing the ball at a random position of the arena and wait for it to reach a steady-state with zero velocity. Its position was the same for different starting positions, and could therefore be measured as a non-changing value. The distance of the ball from the plate center could therefore be computed in order to evaluate the network performance during learning (see figure-32). One can notice that after $1200s$ of learning, the ball is always stabilised at a distance which is less than 10% of the maximal distance $r_{arena} - r_{ball}$.

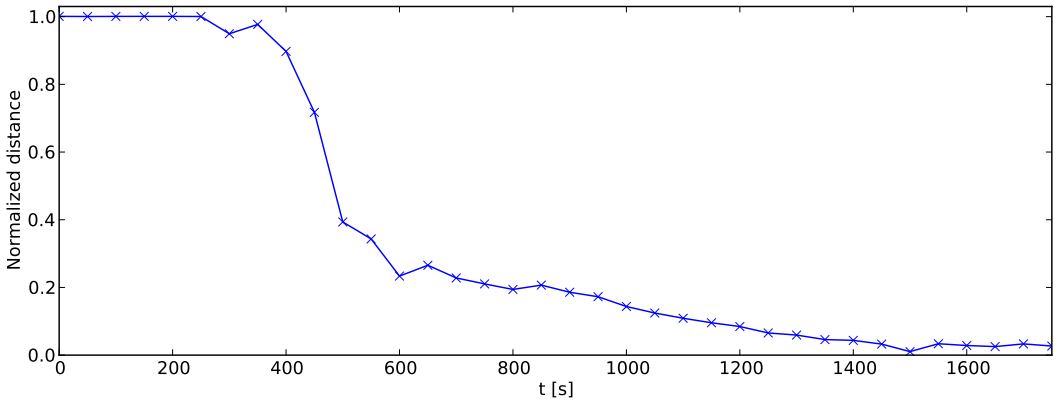

Figure 32: Normalized final distance of the ball from the plate center at different steps of the learning procedure.

The trajectory and speed of the ball during the performing of the task once it was learned, is shown in figure-33.

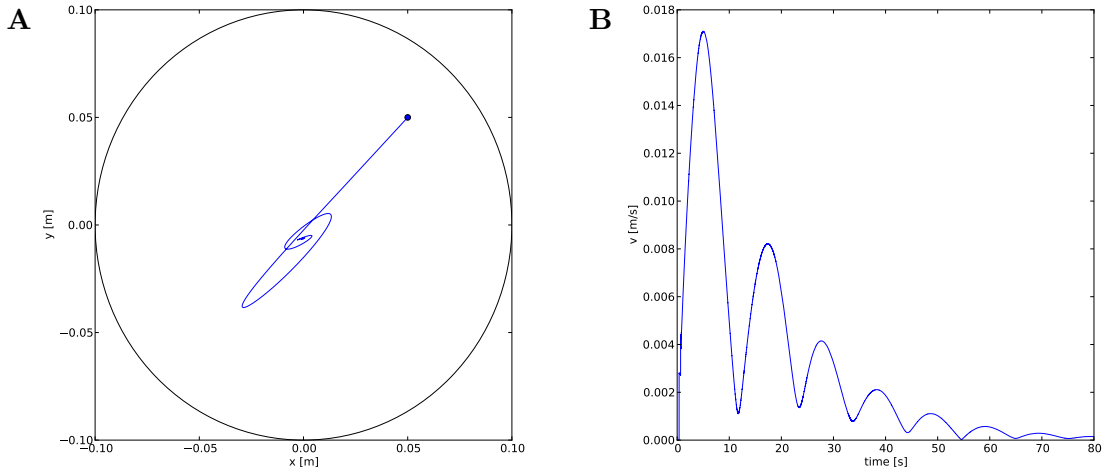

Figure 33: (**A**) Trajectory of the ball in the arena and (**B**) its speed during task performing, starting from a random position, for the 65 mean-field populations.

8.5 Feedback to the column

The main goal of this section is to demonstrate that not only could the weights of the cortical point-neuron column be extracted and plugged into the mean-field model in order to imitate its behavior, but also the opposite was possible. The weights of the mean-field network were therefore taken out after learning, and transformed into conductances by reversing equation-17:

$$\bar{g} = \frac{J \cdot N_{post}}{(E_{e/i} - \bar{V}) \cdot \tau_{syn,e/i} \cdot M_{sy}} \tag{25}$$

The computed conductances were then put back into the cortical point-neuron column, with every synapse between the same pre-and post-populations having the same conductance value.

Since the short-term reaction of the point-neuron column was very different from the mean-field populations in a time interval shorter than $T_{diff} \approx 1000ms$, the kinetics of the ball had to be slower than this period. While this was the case with the arena parameters used (see table-10), it showed that the mean-field model approximation was only valid in a certain range of time. If certain parameters such as the scaling factor for plate orientation S, were changed to provide faster kinetics to the physical system, the point-neurons were not able to execute the task anymore.

For slower kinetics, while the column was able to balance the ball when dropped from the same starting position as previously (see figure-34), its trajectory was different from the previous one. The main reason for this is the error on the mean-field prediction, which combined with a chaotic physical system resulted in a great deviation of the ball from its previous path.

The mere fact, however, that the point-neuron column could accomplish the balancing task in the same time duration as the mean-field populations, validated the calibration and proved the usefulness of this approach. The trajectory and speed of the ball during the performing of the task is shown in figure-34.

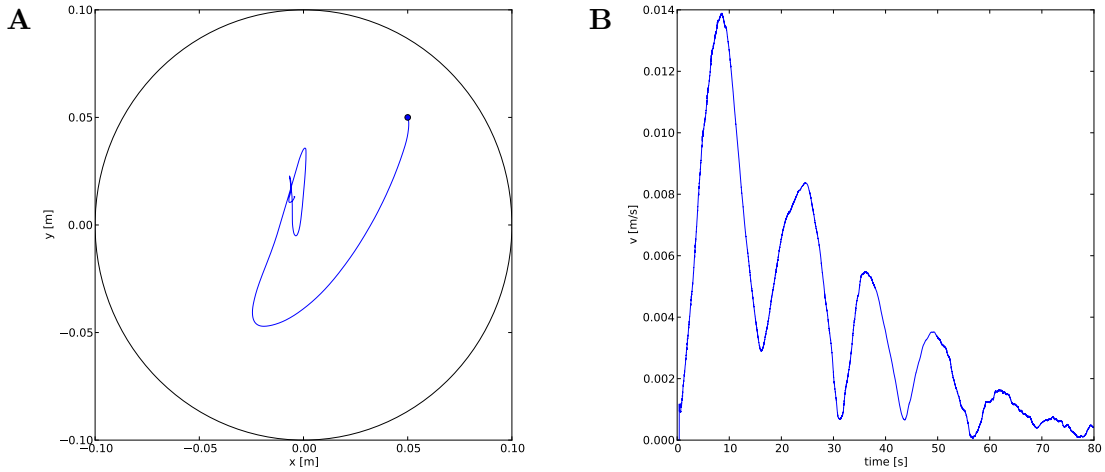

Figure 34: (**A**) Trajectory of the ball in the arena and (**B**) its speed during task performing, starting from a random position, for the cortical point-neuron column with the computed conductances taken from the mean-field network.

9 Discussion

In this project, a method was developed to allow the reduction of a complex biological neural network into a much smaller number of mean-field populations. It developped the tools needed to do so, and pointed out the different problems encountered during the process. It also illustrated the ability to teach a simple task to the column, by simply teaching it first to the mean-field network.

The first issue of the calibration of the mean-field populations was the inability of the current and rate based activation function to take in account not only short-term behaviors of the neurons, but also the change in the synaptic input strength due to the deformation of the membrane potential distribution $P(V)$ of neurons. While this effect was first thought to be neglectable, it turned out to be responsible for a large loss in precision in the approximations of the final rates. Furthermore, its effect was unpredictable due to its non-linearity with the synaptic input currents. This demonstrated one of the flaws of the mean-field model used.

While the mean-field model offered a decent approximation for steady-state rates of neuronal populations, it was not well suited to compute immediate responses, due to the chaotic behavior of the AdEx model. When reducing a point-neuron network, it is therefore vital to determine whether the immediate reaction of certain populations is required or not.

Another limitation of any mean-field model in general, is due to the reduction of the synapse diversity between populations. Getting rid of the variance of the synaptic parameters distribution by reducing them resulted in a great loss of accuracy on the prediction of the column behavior. This was not due to the actual mean-field model itself but rather to the fact of neglecting a considerable part of the information about the biological network. A way of removing this problem would be to develop a method which would replace the arithmetic mean of the synaptic variables by a weighted mean leading to a better approximation of the synaptic variables.

References

[1] Abbott L, Varela J., Sen K., Nelson S. (1997) *Synaptic Depression and Cortical Gain Control* . Science 275, 221 (1997); DOI: 10.1126/science.275.5297.221

[2] Brunel N. (2000) *Dynamics of Sparsely Connected Networks of Excitatory and Inhibitory Spiking Neurons* . Journal of Computational Neuroscience May 2000, Volume 8, Issue 3, pp 183-208

[3] Barak O., Tsodyks M. (2007) *Persistent Activity in Neural Networks with Dynamic Synapses* . PLoS Comput Biol 3(2): e35. doi:10.1371/journal.pcbi.0030035

[4] Brette R., Gerstner W. (2005) *Adaptive Exponential Integrate-and-Fire Model as an Effective Description of Neuronal Activity* . J Neurophysiol 94: 3637–3642, 2005. First published July 13, 2005; doi:10.1152/jn.00686.2005.

[5] Fuhrmann G., Segev I., Markram H., Tsodyks M. (2001) *Coding of Temporal Information by Activity-Dependent Synapses* . J Neurophysiol 87: 140 –148, 2002; 10.1152/jn.00258.2001.

[6] Goldman M., Maldonado P., Abbott L. (2002) *Redundancy Reduction and Sustained Firing with Stochastic Depressing Synapses* . The Journal of Neuroscience, January 15, 2002, 22(2):584–591

[7] Gupta A., Wang Y., Markram H. (2000) *Organizing Principles for a Diversity of GABAergic Interneurons and Synapses in the Neocortex* . Science 287, 273 (2000); DOI: 10.1126/science.287.5451.273

[8] Lefort S., Tomm C., Sarria F., Petersen C. (2008) *The Excitatory Neuronal Network of the C2 Barrel column in Mouse Primary Somatosensory Cortex* . Neuron 61, 301–316 DOI 10.1016/j.neuron.2008.12.020

[9] Lubke J., Feldmeyer D. (2007) *Excitatory signal flow and connectivity in a cortical column: focus on barrel cortex* . Brain Struct Funct, DOI 10.1007/s00429-007-0144-2

[10] Potjans T., Diesmann M., (2011) *The cell-type specific connectivity of the local cortical network explains prominent features of neuronal activity* . arXiv:1106.5678v1 [q-bio.NC] 28 Jun 2011

[11] Probst D. (2012) *Towards Intelligent Avatar Control - Controlling a Ball on a Flat Bounded Arena*

[12] Ramaswamy S., Müller E., Keller D., King J. G. , Hill S. L. , Schürmann F., Markram H.. *A Unifying Model of the Neocortical column* . Program No. 268.10. 2012 Neuroscience Meeting Planner. New Orleans, LA: Society for Neuroscience, 2012. Online.

[13] Schmidl H. and Milenkovic V. J. (2004) *A Fast Impulsive Contact Suite for Rigid Body Simulation* . IEEE TRANSACTIONS ON VISUALIZATION AND COMPUTER GRAPHICS, VOL. 10, NO. 2, MARCH/APRIL 2004

[14] Shriki O., Hansel D., Sompolinsky H. (2003) *Rate Models for Conductance-Based Cortical Neuronal Networks* . Neural Computation 15, 1809–1841

[15] Sussillo D., Toyoizumi T., Maass W. (2007) *Self-Tuning of Neural Circuits Through Short-Term Synaptic Plasticity* . J Neurophysiol 97:4079-4095, 2007. First published 4 April 2007; doi: 10.1152/jn.01357.2006

[16] Tsodyks M., Markram H. (1997) *The neural code between neocortical pyramidal neurons depends on neurotransmitter release probability* . Proc. Natl. Acad. Sci. USA, Vol. 94, pp. 719–723, January 1997 Neurobiology

[17] Tsodyks M., Pawelzik K., Markram H. (1997) *Neural Networks with Dynamic Synapses* Neural Computation 10, 821–835 (1998) .

[18] `http://matplotlib.org/`

[19] `http://www.nest-initiative.org/index.php/PyNEST`

[20] `http://www.numpy.org/`

[21] `http://www.opengl.org/`

[22] `http://www.scipy.org/`

[23] `http://www.libsdl.org/`

10 Appendix

10.1 Mean-field equations Euler method

The mean-field equations were computed with the Euler method for M populations as shown below.

```
# backing up variables so that they stay unchanged
# available resources
x_old = np.copy(x)
# synaptic efficacy
U_1_old = np.copy(U_1)
# rate
F_old = np.copy(F)
# update variables
x   += dt*((1.0-x_old)/tau_rec - (U_1_old*(1.0-U_0)+U_0)*x_old
       *np.resize(F_old.T, (M,M)) )
U_1 += dt*(-U_1_old*(1.0/tau_fac) + U_0*(1.0-U_1_old)
       *np.resize(F_old.T, (M,M)) )
F   += dt*(1.0/tau_syn)*(-F_old
       +h( np.dot(J*x_old*(U_1_old*(1.0-U_0)+U_0),F_old) +I_ext(t)))
```

10.2 Mean-field equations Runge-Kutta 4 method

The mean-field equations were computed with the Runge-Kutta 4 method for N populations as shown below.

```
# backing up variables so that they stay unchanged
# available resources
x_old = np.copy(x)
# synaptic efficacy
U_1_old = np.copy(U_1)
# rate
F_old = np.copy(F)

# computation of the 4 Runge-Kutta terms

dU1 = (-(U_1_old)*(1.0/tau_fac) + U_0*(1.0-(U_1_old))
      *np.resize(F_old.T, (M,M)) )
dx1 = ((1.0-(x_old))/tau_rec - fct_U(U_1_old, U_0)*(x_old)
      *np.resize(F_old.T, (M,M)) )
dF1 = (1.0/tau_syn)*(-(F_old)
      + h( np.dot(J*x_old*fct_U(U_1_old, U_0),(F_old)) + I_ext(t)))

dU2 = (-(U_1_old+0.5*dt*dU1)*(1.0/tau_fac)
      + U_0*(1.0-(U_1_old+0.5*dt*dU1))
      *np.resize((F_old+0.5*dt*dP1).T, (M,M)) )
dx2 = ((1.0-(x_old+0.5*dt*dx1))/tau_rec
      - fct_U((U_1_old+0.5*dt*dU1), U_0)
      *(x_old+0.5*dt*dx1)*np.resize((F_old+0.5*dt*dP1).T, (M,M)) )
dF2 = (1.0/tau_syn)*(-(F_old+0.5*dt*dP1)
      + h( np.dot(J*(x_old+0.5*dt*dx1)
      *(U_1_old+0.5*dt*dU1*(1.0-U_0)+U_0),(F_old+0.5*dt*dP1))
```

```
      + I_ext(t)))

dU3 = (-(U_1_old+0.5*dt*dU2)*(1.0/tau_fac)
      + U_0*(1.0-(U_1_old+0.5*dt*dU2))
      *np.resize((F_old+0.5*dt*dP2).T, (M,M)) )
dx3 = ((1.0-(x_old+0.5*dt*dx2))/tau_rec
      - fct_U((U_1_old+0.5*dt*dU2), U_0)
      *(x_old+0.5*dt*dx2)*np.resize((F_old+0.5*dt*dP2).T, (M,M)) )
dF3 = (1.0/tau_syn)*(-(F_old+0.5*dt*dP2)
      + h( np.dot(J*(x_old+0.5*dt*dx2)
      *(U_1_old+0.5*dt*dU2*(1.0-U_0)+U_0),(F_old+0.5*dt*dP2))
      + I_ext(t)))

dU4 = (-(U_1_old+1.0*dt*dU3)*(1.0/tau_fac)
      + U_0*(1.0-(U_1_old+1.0*dt*dU3))
      *np.resize((F_old+1.0*dt*dP3).T, (M,M)) )
dx4 = ((1.0-(x_old+1.0*dt*dx3))/tau_rec
      - fct_U((U_1_old+1.0*dt*dU3), U_0)
      *(x_old+1.0*dt*dx3)*np.resize((F_old+1.0*dt*dP3).T, (M,M)) )
dF4 = (1.0/tau_syn)*(-(F_old+1.0*dt*dP3)
      + h( np.dot(J*(x_old+1.0*dt*dx3)
      *(U_1_old+1.0*dt*dU3*(1.0-U_0)+U_0),(F_old+1.0*dt*dP3))
      + I_ext(t)))

# update variables
U_1 += (dt/6.0)*(dU1+2.0*dU2+2.0*dU3+dU4)
x   += (dt/6.0)*(dx1+2.0*dx2+2.0*dx3+dx4)
F   += (dt/6.0)*(dF1+2.0*dF2+2.0*dF3+dF4)
```

10.3 Impulse based collision response of the plate

The approach of impulse based collision responses is to use the impulse term defined as

$$\vec{j} = \int_{t_0}^{t_1} \vec{f} \cdot dt$$

$\vec{f}$ being the force that acts on an object during collision (from time t_0 to t_1) with a static obstacle. This approach allows to compute directly the change of velocity after a collision of 2 objects, instead of applying forces during multiple timesteps which would result in many imprecisions and instabilities.

For an object without rotation and a static obstacle, the norm of the impulse can be written as

$$\|\vec{j}\| = -(1+e) \cdot (\vec{v} \cdot \vec{n}) \cdot m$$

e being the coefficient of restitution, m the mass of the object, $\vec{v}$ the velocity of the object and $\vec{n}$ the normal vector at the collision point, perpendicular to the obstacle.

Finally, the velocity of the object is directly updated as

$$\vec{v}(t+\Delta_t) = \vec{v}(t) - \frac{\|\vec{j}\|}{m} \cdot \vec{n}$$

The described equations are a simplified form of the global impulse equations (Schmidl H. and Milenkovic V. J. 2004), since they don't take any rotation in account and one of the 2 collision objects is always static.

10.4 Synaptic constant standard-deviations

The values of standard-deviations of the synaptic values between the 55 populations are as follows.

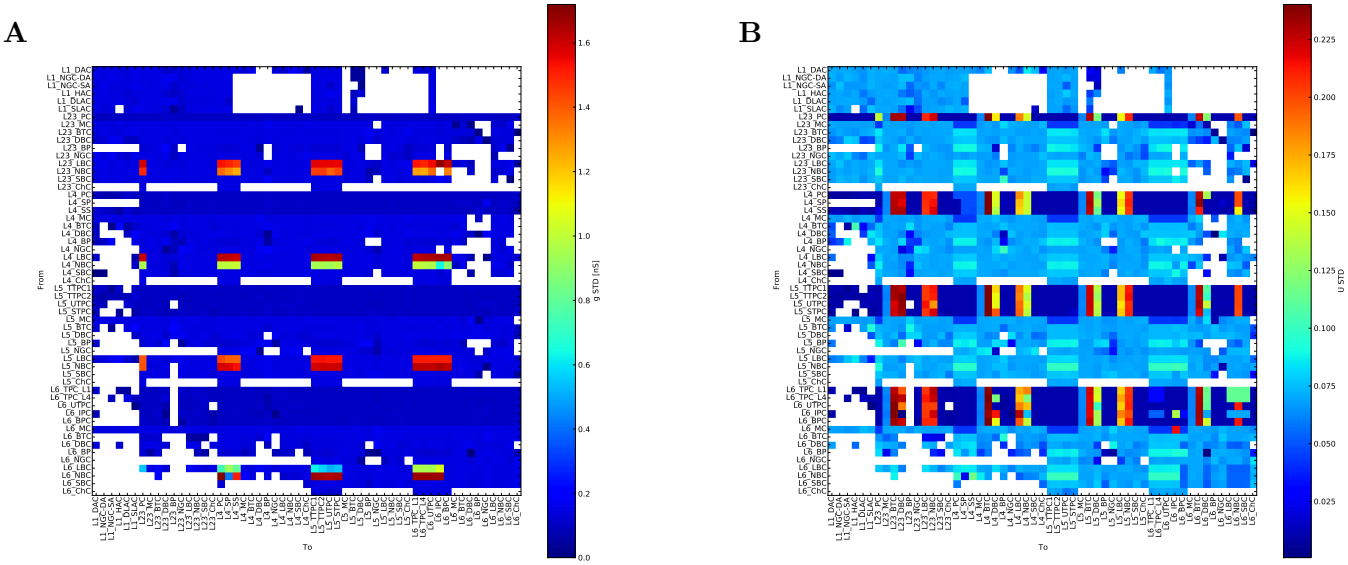

Figure 35: Standard-deviation of (**A**) synaptic conductances and (**B**) synaptic efficacy increases between the 55 different populations.

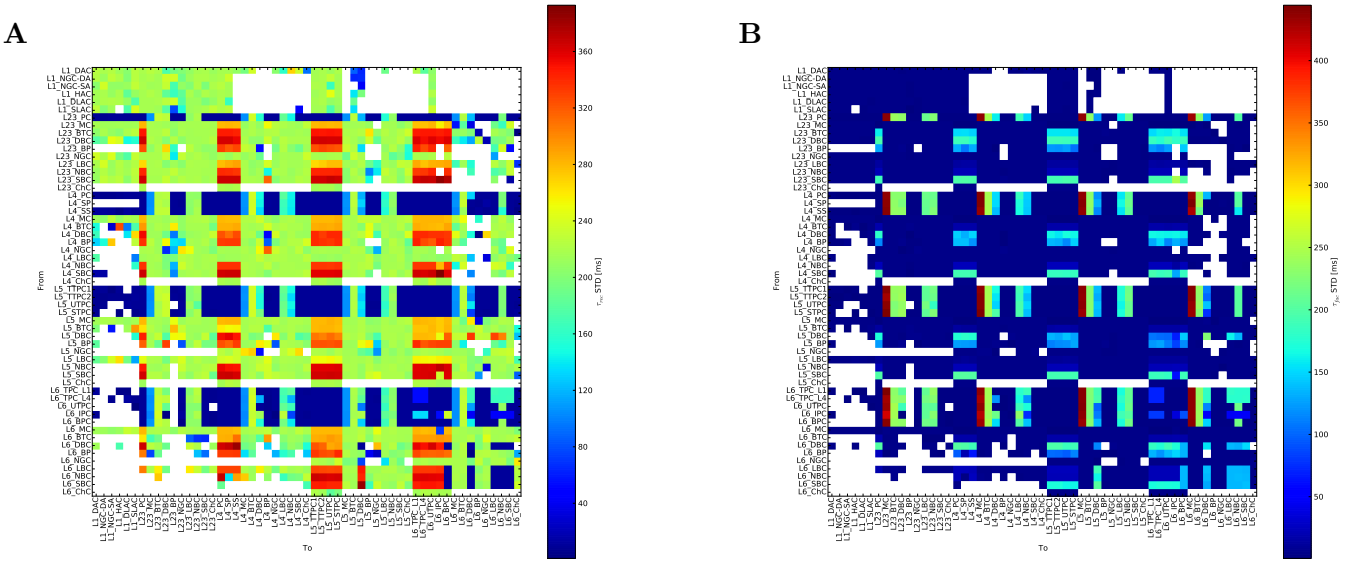

Figure 36: Standard-deviation of synaptic (**A**) recovery time constants and (**B**) facilitating time constants between the 55 different populations.